Nano Energy 122 (2024) 109316

Contents lists available at ScienceDirect

Nano Energy

journal homepage: www.elsevier.com/locate/nanoen

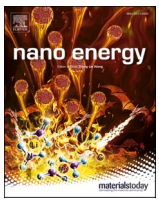

Review

Advances in Self-powered Triboelectric Sensor toward Marine IoT

Yongjiu Zou [a], Minzheng Sun [a], Shuang Li [a], Xinyu Zhang [a], Liang Feng [b], Yu Wang [b], Taili Du [a,*], Yulong Ji [c], Peiting Sun [c], Minyi Xu [a,*]

[a] Dalian Key Lab of Marine Micro/Nano Energy and Self-Powered Systems, Marine Engineering College, Dalian Maritime University, Dalian 116026, China
[b] CAS Key Laboratory of Separation Sciences for Analytical Chemistry, Dalian Institute of Chemical Physics, Chinese Academy of Sciences, Dalian 116023, China
[c] Marine Engineering College, Dalian Maritime University, Dalian 116026, China

ARTICLE INFO

Keywords:
Triboelectric nanogenerators
Self-powered sensor
Energy conversion
Marine Internet of Things

ABSTRACT

With the rapid advances of electronics/materials and manufacturing, marine sensors have made significant progress in the field of ship and ocean engineering, which could cater to the development trend of marine Internet of Things (MIoT) and intelligent ship. As the number of marine sensors increases and the range of distribution expands, developing a continuous, sustainable, and ubiquitous power source is critical for ocean sensing, but it is an unsolved scientific challenge. Marine self-powered sensing through triboelectric nanogenerators (TENGs) may be a promising approach to this emergency. TENG can efficiently convert mechanical triggers from the surrounding environment into electrical signals. It has the advantages of highly efficient mechanical-to-electrical energy conversion, self-sustainability, broad material availability, low cost and good scalability. This article reviews the working principle of marine triboelectric sensors and their applications in the field of ship and ocean engineering. They are mainly divided into five categories: tactile sensor, displacement sensor, flow sensor, vibration sensor and velocity sensor, involving their advanced structure designs, functional material innovations and marine application scenarios. Finally, we highlight the academic challenges and future prospects of these technologies, as well as the key points to be considered in transforming them into commercial applications.

1. Introduction

In recent years, relying on intelligent ocean engineering, it is very critical to accelerate the construction of marine three-dimensional (3D) monitoring network while promoting the development of intelligent ships and upgrading the marine industries [1–5]. Due to the advantages of low cost and high automation, marine sensor networks have been widely used in hydrological information collection [6–10], ship condition monitoring [11–15], marine environmental monitoring [16–21], maritime safety monitoring [22–25] and other fields [26–30].Through the continuous development in recent years, the application of marine sensor networks in the field of ship and ocean engineering has achieved good results and has become the main means for marine information collection [31–34]. They are gradually developing in the direction of miniaturization, high precision, low energy consumption, and networking to achieve rapid response and diverse scene applications [35–38].

Marine sensor networks are widely distributed in ships [39–43], aquatic [44–47], underwater [48–52], offshore platforms [53–56] and onshore buildings [57–59], including displacement sensors, temperature sensors, flow sensors, vibration sensors, speed sensors, pressure sensors and tactile sensors. However, the biggest challenge for developing the existing marine sensor networks is that the battery life of traditional power supply methods is limited, and batteries need to be replaced or charged regularly, which will not only lead to inconvenience in maintenance but also additional maintenance consumption, especially in the case of such a large distributed marine sensor network [60–64]. In addition, most battery systems are manufactured with toxic chemicals, which may pose potential risks to the marine environment [65–68]. Therefore, such marine sensor networks urgently need universal, sustainable and environmentally friendly energy alternatives [69–73].

In 2012, Professor Wang Zhonglin first proposed the triboelectric nanogenerator (TENG) based on the conjunction of triboelectrification and electrostatic induction, which is a new energy conversion method based on Maxwell's theory [74–78]. TENG has the

* Corresponding authors.
E-mail addresses: dutaili@dlmu.edu.cn (T. Du), xuminyi@dlmu.edu.cn (M. Xu).

https://doi.org/10.1016/j.nanoen.2024.109316
Received 9 November 2023; Received in revised form 13 January 2024; Accepted 17 January 2024
Available online 20 January 2024

advantages of simple structure, light weight, low cost, wide range of material selection and strong environmental compatibility, and has obvious advantages in the field of self-powered sensing technology [79–84]. TENG can directly convert different types of mechanical motion into electrical signals with high signal-to-noise ratio, perceive the marine environment parameters and the working state parameters of ship system and equipment, realize the self-powered sensing of motion perception signals in the field of ship and ocean engineering, and provide strong data support for intelligent marine sensor networks [85–89]. As a new electromechanical conversion method, TENG has achieved remarkable results in the field of ship and ocean engineering [24, 90–93]. Professor Wang's team from the Beijing Institute of Nanoenergy and Systems has made great contributions to TENG-based vibration monitoring of ship equipment, vibration positioning sensing and marine environment perception [34,94–97]. Professor Xu's team from Dalian Maritime University has conducted extensive research on wave sensing in marine environment and tactile sensing of underwater robots [98–102]. Professor ding's team of Tsinghua University systematically analyzed the output characteristics of TENG under high-frequency mechanical gearbox vibration, and successfully realized a variety of fault detection of mechanical gearbox [103–107]. Professor cheng's team of Changchun University of Technology has achieved many achievements

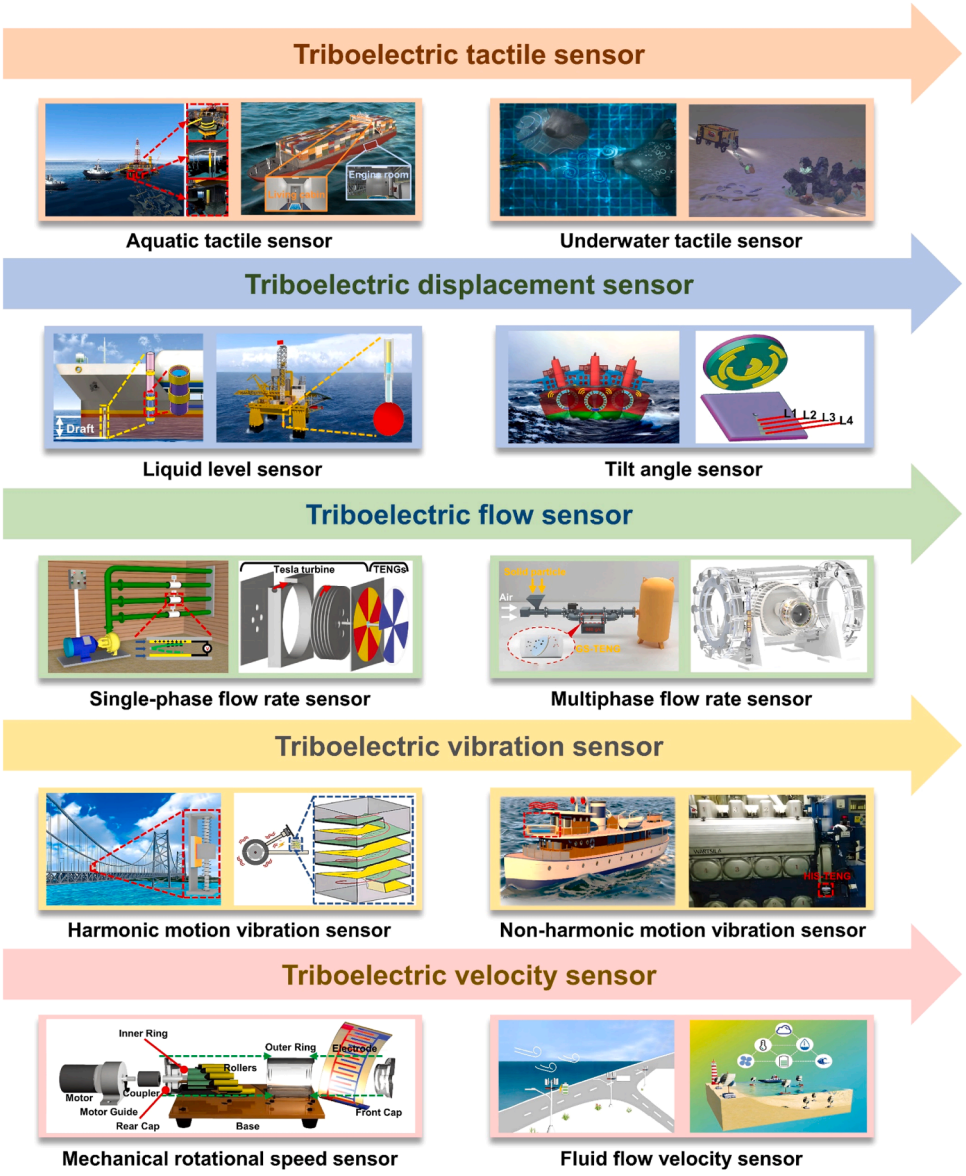

Fig. 1. Classification of marine self-powered triboelectric sensors. Aquatic tactile sensor (Reproduced with permission from ref [101]. Copyright 2022 Elsevier. Reproduced with permission from ref [138]. Copyright 2022 American Chemical Society); Underwater tactile sensor (Reproduced with permission from ref [139]. Copyright 2022 Elsevier. Reproduced with permission from ref [117]. Copyright 2022 The Nature Publishing Group); Liquid level sensor (Reproduced with permission from ref [100]. Copyright 2019 Wiley-VCH. Reproduced with permission from ref [140]. Copyright 2020 American Chemical Society); Tilt angle sensor (Reproduced with permission from ref [99]. Copyright 2020 Elsevier. Reproduced with permission from ref [141]. Copyright 2015 Wiley-VCH); Single-phase flow rate sensor (Reproduced with permission from ref [142]. Copyright 2020 MDPI. Reproduced with permission from ref [143]. Copyright 2019 Wiley-VCH); Multiphase flow rate sensor (Reproduced with permission from ref [144]. Copyright 2021 Wiley-VCH. Reproduced with permission from ref [108]. Copyright 2022 American Chemical Society); Harmonic motion vibration sensor (Reproduced with permission from ref [145]. Copyright 2020 American Chemical Society. Reproduced with permission from ref [146]. Copyright 2017 Wiley-VCH); Non-harmonic motion vibration sensor (Reproduced with permission from ref [147]. Copyright 2022 MDPI. Reproduced with permission from ref [11]. Copyright 2019 Wiley-VCH); Mechanical rotational speed sensor (Reproduced with permission from ref [148]. Copyright 2018 Wiley-VCH); Fluid flow velocity sensor (Reproduced with permission from ref [149]. Copyright 2022 American Chemical Society. Reproduced with permission from ref [150]. Copyright 2023 Wiley-VCH).

in the research of fluid flow sensor and liquid level sensor in pipeline [108–112]. Professor Yang's team from Southwest Jiaotong University demonstrated the liquid-metal based triboelectric acceleration sensor, which can measure the vibration of mechanical equipment in real time [14,113,114]. Specifically, the existing triboelectric marine sensors can be classified into five types according to their application scenarios and sensing information: triboelectric tactile sensors [11,115–117], triboelectric displacement sensors [118–122], triboelectric flow sensors [123–127], triboelectric vibration sensors [128–132] and triboelectric velocity sensors [133–137]. The specific classification is shown in Fig. 1.

In this article, the application of marine triboelectric sensor as an emerging technology in state parameter perception in the field of ship and ocean engineering is systematically studied and introduced for the first time. Specifically, we focus on the structural design, working principle, and application of marine triboelectric sensors, which are a subset of marine triboelectric nanogenerators, but have not been systematically reviewed before. We first illustrate the working mechanism of TENG and introduce the working principle of triboelectric sensor, including tactile sensors, displacement sensors, flow sensors, vibration sensors and velocity sensors. Next, we comprehensively review each class of marine triboelectric sensors from the perspective of functional material innovations, advanced structure designs, marine application scenarios and the potential benefits of integrating artificial intelligence technologies. Finally, we offer an overview of exsisting challenges that limit the extensive application of these technologies and suggest some future directions for mitigating them. This review will significantly drive the development of marine self-powered triboelectric sensor, which will soon revolutionize the upcoming intelligent and green ship and ocean engineering in the era of Marine Internet of Things (MIoT).

2. Fundamental Mechanism of Marine Triboelectric Sensors

2.1. Theory of triboelectric nanogenerators

Since the TENG was first proposed by Professor Wang's team in 2012, the TENG has developed four main operating modes: contact-separation mode, lateral sliding mode, single-electrode mode and free-standing triboelectric-layer mode [151]. As one of the most basic and common working modes (Fig. 2i), the contact-separation mode is widely used in various marine sensors mentioned in this paper. To better explain the principle of TENG in moving media systems, Wang's team has recently successfully derived the dynamic Maxwell equations in non-uniform moving media systems [74], which can well describe the evolution law of electromagnetic field when charged solid and fluid media move at any speed [77,152]. At the same time, the addition of P_S in the term D' successfully introduces the contribution of electrostatic charge caused by contact charging, indicating that the triboelectric charge is generated by the physical contact between two different materials, independent of the presence of electric field, which effectively explains the triboelectrification principle of moving objects in a moving medium system.

$$\nabla \cdot D' = \rho_f - \nabla \cdot P_S \tag{1}$$

$$\nabla \cdot B = 0 \tag{2}$$

$$\nabla \times E = -\left(\frac{\partial}{\partial t} + v \cdot \nabla\right) B \tag{3}$$

$$\nabla \times H = J_f + \left(\frac{\partial}{\partial t} + v \cdot \nabla\right)\left(P_S + D'\right) \tag{4}$$

Where D' is the electric displacement field, ρ_f is the free charge density, P_S is the polarization density term in the displacement vector, representing the polarization owing to the pre-existing electrostatic charges on the medium, B is the magnetic field, E is the electromagnetic field, v is the translation velocity, H is the magnetizing field, J_f is the local free electric current density, which primarily expand the applications of TENG in various fields.

The electron cloud/potential model based on electron cloud interaction can also further explain the microscopic process of charge transfer between different material contacts in a moving media system [153–156]. The electrons within an atom or molecule are bound to their original orbitals, forming a cloud of electrons (Fig. 2ii). When driven by different types of mechanical movements in the marine environment, different materials contact each other, the distance between the electron clouds decreases, and eventually, the electron clouds overlap, the interatomic barrier decreases, and the electron jump occurs. On a macro level, opposite charges appear on the contact surface of different materials, forming a potential difference, and then generate an electrical signal.

2.2. Theory of marine triboelectric sensors

In the field of ship and ocean engineering, it has a variety of motion modes such as flow, vibration, rotation, etc., which can promote

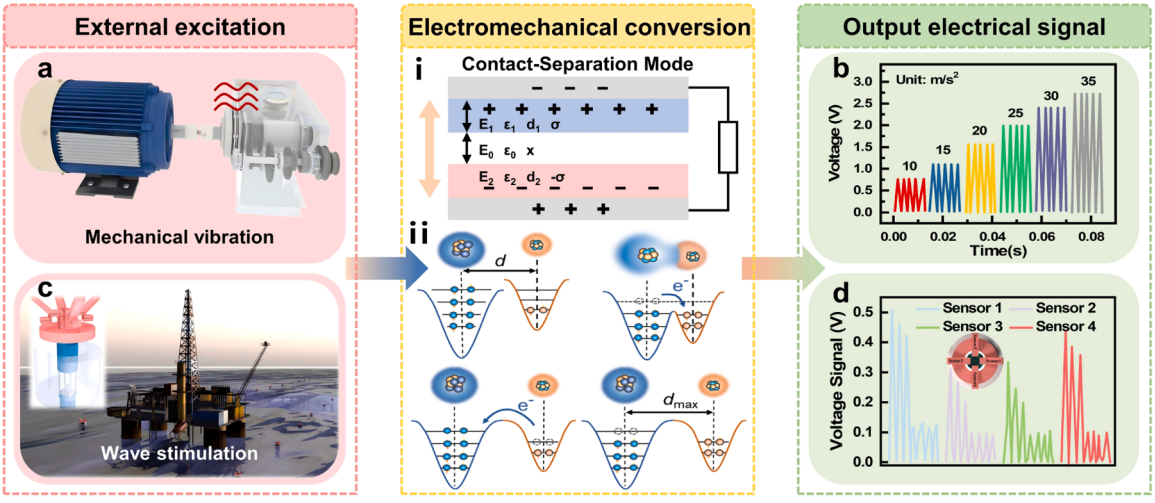

Fig. 2. Flow chart of working principle of marine triboelectric sensor. Reproduced with permission from ref [154]. Copyright 2020 Elsevier. (a) Application Scenarios of VS-TENG. (b) Voltage signals under different accelerations. Reproduced with permission from ref [103]. Copyright 2022 Wiley-VCH. (c) Applications of the BCWS in the marine platform. (d) The signal output characteristics of BCWS. Reproduced with permission from ref [102]. Copyright 2021 Wiley-VCH.

alternating contact and separation between different materials through liquid-solid contact, film flapping, tensile deformation, extrusion and other ways [151,152,157–160]. Based on the working principle of the TENG, a potential difference is formed between the two tribo-materials to generate current through the external load circuit [76]. Fig. 2 depicts the process of converting typical mechanical movements in the field of ship and ocean engineering into electrical signals. Through the analysis and processing of electrical signals, the motion information of excitation source can be characterized. Therefore, it is particularly important to design a variety of sensors. Different sensor structures are designed according to different external excitation ways, so that the two tribo-materials can form stable and efficient output under the excitation of different motion modes, and realize the effective collection and self-powered sensing of marine information. [161–163] Based on the equivalent physical model shown in Fig. 2i, the electric field intensity of each region obtained by Gauss theorem is given by:

Inside the air gap

$$E_0 = \frac{\sigma(t) - \frac{Q}{S}}{\varepsilon_0} \tag{5}$$

Inside the dielectric layer 1

$$E_1 = \frac{-Q}{\varepsilon_0 \varepsilon_1 S} \tag{6}$$

Inside the dielectric layer 2

$$E_2 = \frac{-Q}{\varepsilon_0 \varepsilon_2 S} \tag{7}$$

Here, E_0, E_1 and E_2 is the electric field strength. t is time, $\sigma_{(t)}$ is the surface charge density varying with time; ε_0 is the permittivity in a vacuum; Q is the amount of transferred charge; S is the surface area of the metal electrode. $\varepsilon_1$and ε_2 are the relative dielectric constant of the dielectric layer [154].

The voltage between the two electrodes can be given by

$$V = E_0 \bullet x + E_1 \bullet d_1 + E_2 \bullet d_2 \tag{8}$$

Therefore, the *V-Q-x* relationship of TENG in the motion system can be obtained as follows:

$$V = \frac{-Q}{\varepsilon_0 \bullet S}\left(x(t) + \frac{d_1}{\varepsilon_1} + \frac{d_2}{\varepsilon_2}\right) + \frac{\sigma x(t)}{\varepsilon_0} \tag{9}$$

where x is the air gap distance between two tribo-materials, $x(t)$ is the time-varying distance between two tribo-materials in the motion system, d_1, and d_2 represent the thickness of two tribo-materials [164,165].

In the theory, when TENG is used as a sensor, the output voltage value is generally used as the sensing signal. However, faced with a complex sensing environment, the TENG sensor with weak performance will have a low signal-to-noise ratio, which makes it impossible to perceive more comprehensive information. Therefore, it is necessary to improve the performance of TENG. Through the theoretical formula 9, we can know that changing the tribo-materials can optimize the relative dielectric constant and surface charge density, alter the material area and the gap of the tribo-materials, so as to promote the output performance of TENG, obtain a higher signal-to-noise ratio for the output signal, and better facilitate the environmental perception ability of TENG [166–168].

3. Marine Triboelectric Sensors

Recently, researchers have made great efforts to develop marine triboelectric sensors that can sense the marine environment as well as the state of mechanical equipment without the need for an external power source. Under the external excitation, the internal structure of the TENG will produce corresponding mechanical movement, resulting in alternating contact and separation between the two tribo-materials, thus converting the external excited mechanical movement into electrical signals. Different types of mechanical excitation, such as vibration, flapping, flow, rotation and touch, have different mechanical motion characteristics, so the structural design and tribo-material selection of TENG are also different. Therefore, according to the different functions of the sensors, the marine triboelectric sensors are mainly divided into five categories: tactile sensors, displacement sensors, flow sensors, vibration sensors and speed sensors.

3.1. Triboelectric tactile sensor

The triboelectric tactile sensor is a passive sensing sensor compared to other sensors, which is often used to detect physical parameters such as pressure and deformation. In the field of marine engineering, it is used in scenes such as environmental information perception [169], human-computer interaction [170,171], underwater grasping [172] and underwater robot collision avoidance [173,174]. By sensing the pressure or deformation of the measured object, the triboelectric tactile sensor is capable of establishing contact and separation between different tribo-materials within the sensor, so as to generate electrical signals and realize the tactile perception of the working state of mechanical equipment or the surrounding environment information. In this paper, according to the different spatial dimensions of the application scenario, the triboelectric tactile sensor is divided into two categories: aquatic triboelectric tactile sensor and underwater triboelectric tactile sensor.

3.1.1. Aquatic tactile sensor

Aquatic tactile sensors are mainly used in the status monitoring of marine structures such as ocean platforms and ocean environments [169]. Prolonged exposure to periodic waves, wind and other hazardous loads can lead to damage or even destruction of marine structures. Marine structural health monitoring is dedicated to monitoring the tensile, impact, bending and other mechanical deformation of structures under the action of external forces. Therefore, the monitoring of marine structures through tactile perception is a necessary means to ensure the safety. Firstly, Zhao et al. proposed a highly stretchable rope-like TENG (R-TENG) for monitoring the mechanical loads of marine structures [101]. R-TENG has advantages of excellent stretchability, flexibility and resistance to humidity, which reflect the potential as an attractive marine equipment monitor to prevent collision. Fig. 3a demonstrates the utilization of R-TENG for monitoring marine structure. R-TENG can not only reflect the mooring state of the ship by monitoring the tensile load on the mooring cable, but also monitor the bending load of the lower piping system of the offshore platform and the collision load of the platform legs to monitor the offshore platform in multiple perspectives. As shown in Fig. 3b, R-TENG is composed of a commercial steel spring, a silicone rubber and a latex tube. When the R-TENG is exposed to external stimulation, the latex tube and silicone rubber will alternately contact and separate, thus forming an electric current between the steel spring and the ground. The change of voltage under different pressing force is shown in Fig. 3c. The output voltage exhibits a favorable linear correlation with the pressing force.

For ocean environmental monitoring, a self-powered triboelectric bionic coral wave sensor (BCWS) was proposed for detecting ultra-low frequency and irregular ocean waves [102]. The data obtained by BCWS monitoring the surrounding marine environment can provide effective help for marine infrastructure development, marine resource utilization, and the detection of maritime disasters. Fig. 3d shows the potential application of the BCWS in marine platform monitoring. Multiple BCWSs can be placed uniformly around the marine platform to monitor the ocean waves in all directions, then provide data to the engineer to ensure safe operation of the platform. The working principle of the BCWS is shown in Fig. 3e. When the FEP film is alternately contacted and separated from the conductive ink electrode in oscillating motion, an electrical signal is generated in the external circuit. As shown in

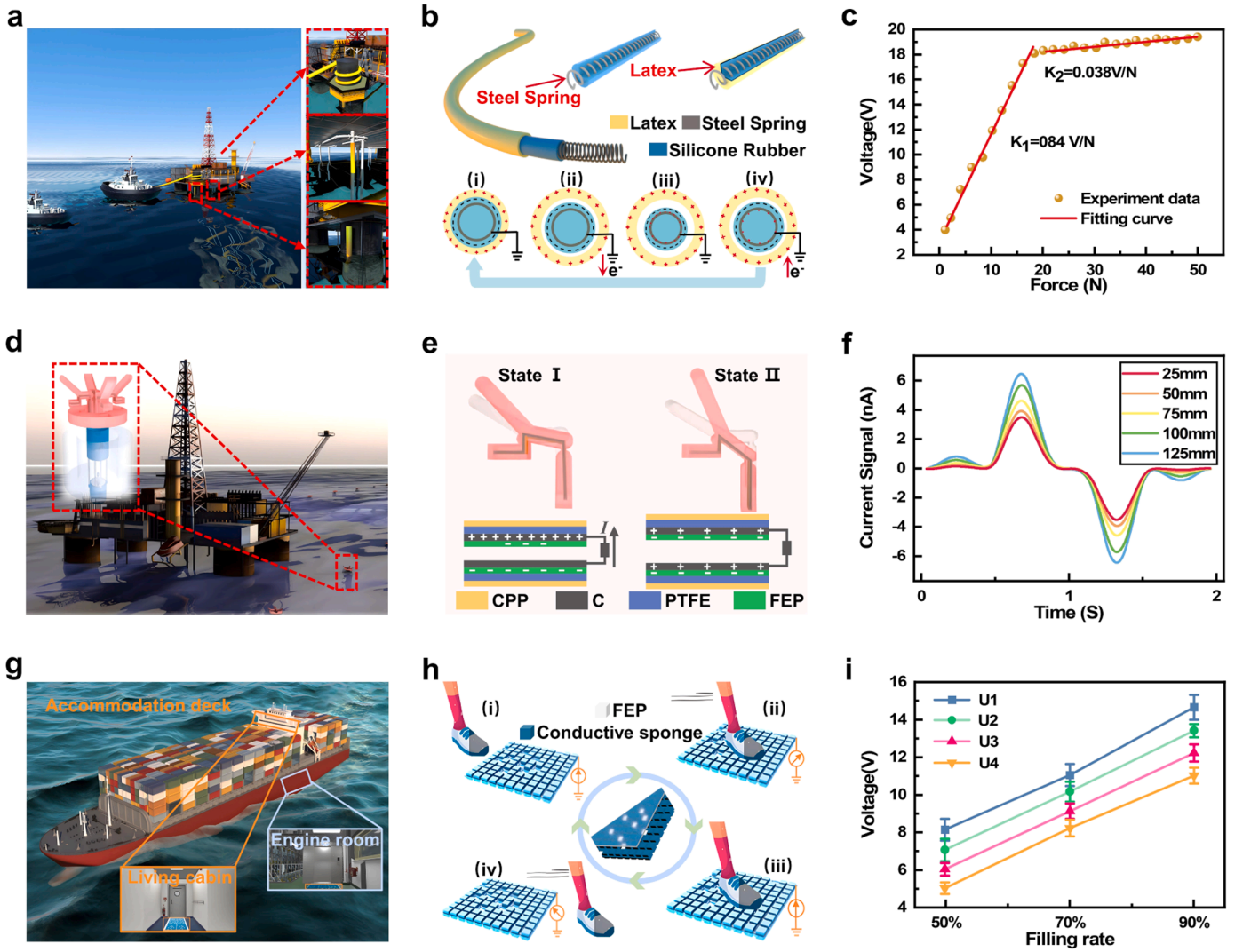

Fig. 3. The triboelectric tactile sensor: Aquatic tactile sensor. (a) R-TENG monitoring map of ocean conditions. (b) The structure and working principle of R-TENG. (c) R-TENG output voltage curve with pressure. Reproduced with permission from ref [101]. Copyright 2022 Elsevier. (d) Application Scenarios of BCWS. (e) Working principle of the BCWS. (f) At w = 0° and f = 0.65 Hz, the dependence of the output current of BCWS on H. Reproduced with permission from ref [102]. Copyright 2021 Wiley-VCH. (g) Application of DL Smart mats. (h) The working mechanism of DL Smart mats. (i) DL Smart mats output voltage variation with fill rate and user. Reproduced with permission from ref [138]. Copyright 2022 American Chemical Society.

Fig. 3f, the output current signal generated by wave stimulation increases with the increase of wave height and have a millimeter-level response to the different wave height. With high precision wave sensing ability, BCWS undoubtedly has great prospects in the field of ocean engineering sensing.

To build the MIoT and ensure personnel safety, Wang et al. proposed a minimalist structure triboelectric smart sensing mat system with deep learning (DL) assistance for the comprehensive monitoring of crew [138]. Application scenarios of the smart sensing mat system are shown in Fig. 3g. Whether the crew is in the living cabin or the closed cabin of the engine room, the smart sensing mat system can realize the comprehensive monitoring of the personnel status. Working principle of the triboelectric smart sensing module unit as shown in Fig. 3h. When a person steps on the mat, the interaction between the fluorinated ethylene propylene (FEP) and the conductive sponge will generate a triboelectric signal according to the principle of contact-separation mode. The amplitude of output signal of the smart sensing mat unit is related to the contact area of the two materials. With the different filling rate of the conductive sponge, the amplitude of the output signal is different. As depicted in Fig. 3i, when users with different weights step on the mat unit with distinct filling rates, the mat outputs a stable signal with obvious difference. The smart sensing mat system not only provides a high-precision recognition method, but also shows great advantages in terms of cost, structure and scalability. It has broad application prospects in the future construction of intelligent ships. On the basis of intelligent sensing mat, Yang and Shi et al. [175,176] have carried out structural optimization array distribution, which reduces the complexity of output terminals and systems, and improves the accuracy to 99% through DL. Moreover, Jin et al. [170] used the machine algorithm training to achieve multi- target tactile perception with an accuracy rate of more than 98%.

3.1.2. *Underwater tactile sensor*

Autonomous underwater vehicle (AUV) has been widely developed and applied because of its outstanding applicability in various industries [177–179]. While existing force/torque measuring instruments may be suitable for the measurement of parameters in the field of marine and ocean engineering, the quantity of tactile sensors explicitly tailored for utilization in marine applications remains comparatively limited. Marine mammals with tactile receptors have the capability to perceive intricate stimuli arising from the surrounding motion environment. Inspired by these, some scholars have made efforts to explore and

achieved some results. Wang et al. designed an underwater triboelectric bionic whisker sensor (UBWS) [139], which can perceive the hydrodynamic trails generated by the motion of underwater objects (Fig. 4a). As shown in Fig. 4b, the structure of the UBWS consists of inner TENG perceiving unit, a silicone follicle (Dragonskin 00–20), and an artificial whisker (polydimethylsiloxane, PDMS). When the artificial whisker deflected under the the vortex pressure difference, the alternating contact and separation between the FEP film and conductive electrodes will generate electrical signals. As shown in Fig. 4c, the ratio of the distance between the fishtail and the UBWS to the characteristic length (D/L) of the UBWS gradually increases from 1 to 5, the pressure difference caused by the vortex gradually dissipates and the output voltage of the UBWS gradually decreases. The UBWS can effectively perceive the eddy current caused by target disturbance. In addition, it could be combined with robotic fish to capture underwater targets, which proves the potential application value of TENG tactile perception in hydrodynamic passive vortex sensing. Zou et al. [180] also designed a tactile sensor that can monitor the attitude of underwater personnel in real-time by using bionic characteristics and imitating the ion channel structure of electric eel cell membrane. Its good tensile fatigue resistance (more than 50,000 times) and underwater performance provide a new way for underwater soft wearable electronic devices. To further optimize the structure, Liu et al. designed a triboelectric bio-inspired whisker sensor (BWS), [181] which can be used as an underwater whisker sensor for underwater robots to avoid reactive obstacles (Fig. 4d). The main components of the BWS include a carbon fiber rod, an epoxy resin base, and four sensing units, as shown in Fig. 4e. When BWS is stimulated by the external environment, the carbon fiber rod will cause the octagonal prism to impact the sensing unit, and the FEP film and the ink layer will alternately contact and separate, thereby generating electrical signals. It can be seen from Fig. 4f that as the contact frequency increases, the short-circuit current of the sensing unit increases from 3.81 nA to 18.6 nA. BWS identifies the direction, position and frequency of the external load by extracting the characteristics of the electrical signals transmitted by the four sensing units, especially in the complex situation where optical and acoustic equipment cannot be used. BWS effectively improves the environmental perception ability of underwater vehicles. Furthermore, Xu et al. [174] also explored deep learning (DL) and underwater 3D l tactile perception technology, which realized multi-directional environmental perception of underwater flow field, and provided strong support for underwater robot to avoid collision and maintain motion attitude.

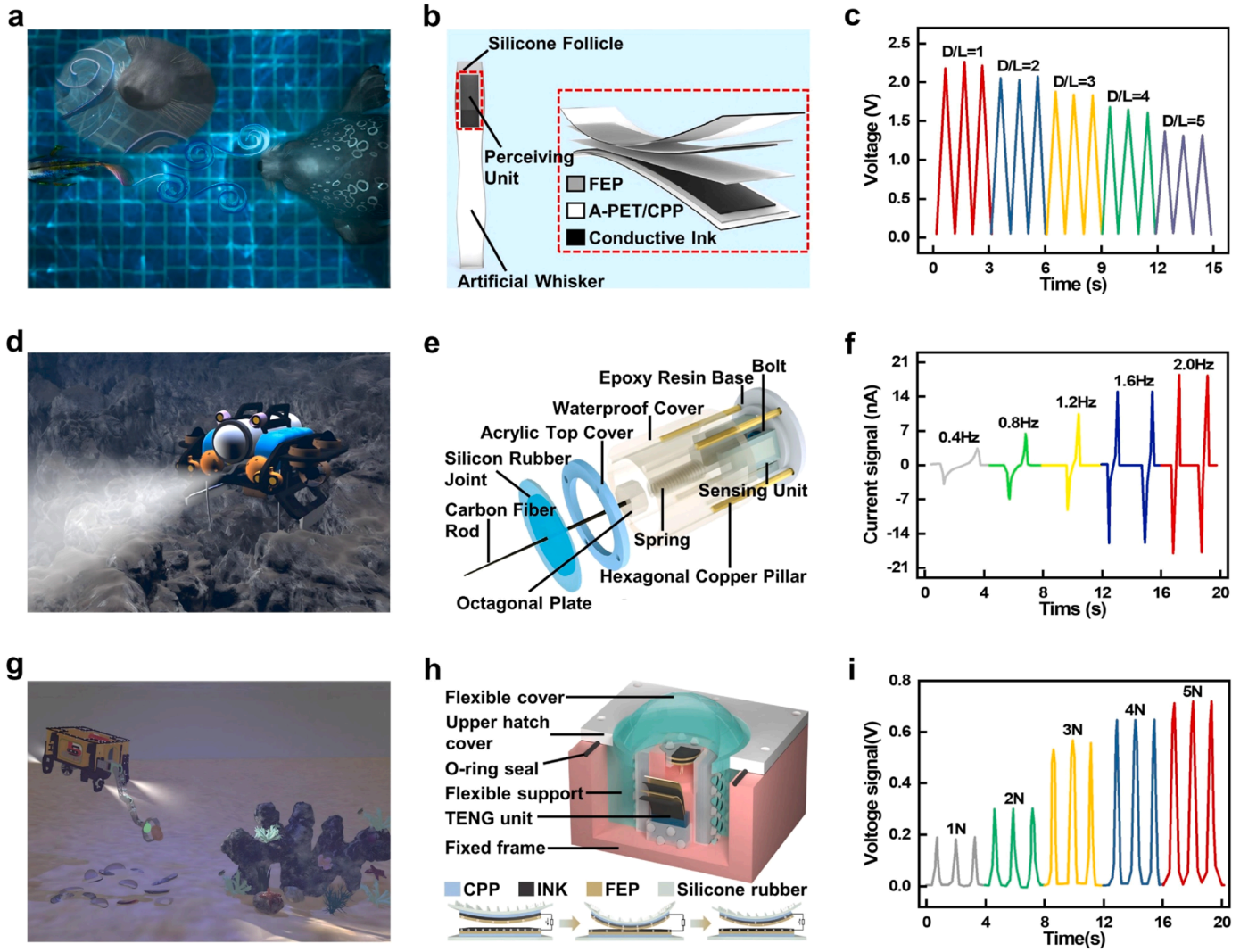

Fig. 4. The triboelectric tactile sensor: underwater tactile sensor.(a) Seals sense targets by the effect of eddy currents on their whiskers. (b) Schematic structure of the UBWS. (c) Curve of UBWS output voltage with D/L value. Reproduced with permission from ref [139]. Copyright 2022 Elsevier. (d) Application Scenarios for BWS. (e) The detailed structure of BWS. (f) Dependence of BWS short-circuit current on external load frequency. Reproduced with permission from ref [181]. Copyright 2022 Elsevier. (g) Schematic diagram of TPTS for signal grabbing. (h) TPTS structure and working principle. (i) TPTS open-circuit voltage when external load changes from 1 N to 5 N. Reproduced with permission from ref [117]. Copyright 2022 The Nature Publishing Group.

Inspired by marine mammals' tactile hunting, Xu et al. developed a self-powered triboelectric palm-like tactile sensor (TPTS) integrated with a tactile sensing system for underwater vehicles [117], which is capable of measuring and distinguishing normal and shear forces generated when touching objects in real time (Fig. 4g). As shown in Fig. 4h, the structure of TENG is made up of triboelectric sensing units, a flexible support unit and a sealing unit. The spine-like structure on the surface of the sensing unit can produce local and high stress concentration near the sensor to enhance pressure perception. When the sensing unit receives an external stimulus, the alternating contact and separation of FEP thin film and ink electrode generates electric signals. When the external load increases from 1 N to 5 N, the TPTS outputs voltage from 0.2 V to 0.7 V, as shown in Fig. 4i. The manipulator integrated with TPTS has the ability to detect the hardness of the sample, and completes a large number of underwater grasping tasks while preventing damage. In addition, Qu et al. [172] have explored materials and developed an environmentally friendly high-performance ion hydrogel with good strain and friction electric tactile sensing capabilities, which effectively improved the active sensing ability of underwater soft robots during grasping.

In short, the triboelectric tactile sensor, as a self-powered sensor that converts tiny mechanical movements into electrical signals using the principle of triboelectric nanogenerators, can sense multi-dimensional information of marine environment and structures with high precision. The sensor has the characteristics of unique structural design, good environmental adaptability, excellent bionic ability, and has shown great application potential in the field of ocean engineering sensing. Compared with acoustic and optical sensors, triboelectric tactile sensors have superior perception performance in underwater information perception, which can realize 3D information perception and eddy current sensing, underwater target acquisition and trajectory perception, and improve the operation capability of underwater equipment. The development of new high-performance materials will also play a great role in improving the active sensing ability of underwater tactile sensors and their integration with soft robots. The introduction of artificial intelligence technology provides more innovation possibilities and application scenarios for triboelectric tactile sensors, which can provide data support for marine ecological protection and resource development, and provide technical means for the early warning and prevention of marine disasters. Through the combination of DL and machine algorithms, intelligent analysis and processing of big data generated by triboelectric tactile sensors are realized, which improves the intelligence level of sensors and provides a way for the construction of MIoT. Through the integration of underwater tactile sensor and underwater robot, the intelligent recognition and tracking of underwater objects can be realized. The safety and efficiency of marine engineering can be ensured by the intelligent monitoring of the health state of marine structures by triboelectric sensors.

3.2. Triboelectric displacement sensor

Triboelectric displacement sensor can sense the relative displacement generated in the motion system. It is often used in the field of marine engineering to perceive the liquid level change caused by ocean wave motion of ships or offshore platforms [182], the inclination change caused by ship swaying [183,184], and the relative displacement caused by mechanical motion [185]. Since it is mainly used to sense the change caused by relative displacement, the existing triboelectric displacement sensor mostly works on the lateral sliding mode, which uses the relative displacement in the moving system to drive the alternating contact and separation between different tribo-materials to generate electrical signals and realize the displacement information perception. According to the different information perceived by the triboelectric displacement sensor, it is divided into two categories: triboelectric liquid level sensor and triboelectric angle sensor.

3.2.1. Liquid level sensor

The triboelectric liquid level sensor is mainly employed for detecting parameters of ship draft and wave height. Compared with traditional liquid level sensors, it possesses the merits of cost-effectiveness, easy installation and no need for external power supply [186]. For the operation mode of solid-liquid contact, Xu et al. first proposed a highly-sensitive triboelectric wave sensor working on liquid-solid interfacing mode (WS-TENG), which could be used for monitoring real-time wave heights [187]. Fig. 5a shows the application of WS-TENG on a marine platform. WS-TENG is fixed to the leg of the platform. When a wave encounters the legs of the platform, WS-TENG can accurately sense the amplitude of the wave. The structure and operational mechanism of WS-TENG is presented in Fig. 5b. WS-TENG is made of polytetrafluoroethylene (PTFE) film covered on a copper electrode. In the initial state, WS-TENG is in charge equilibrium. When the seawater surface changes, the positive charge in contact with the PTFE diaphragm changes accordingly, causing the positive charge on the copper electrode to shift and form a current. Fig. 5c shows a test of WS-TENG in a water tank. WS-TENG is fixed to the legs of a 3D printed platform, when the wave passed over the legs, the peak of the wave was presented on the computer screen. The data obtained indicates the sensitivity of WS-TENG for wave measurement. Detailed data on the wave heights measured by WS-TENG is shown in Fig. 5d. The voltage increases from 0.39 V to 1.98 V during the increase in level height from 10 cm to 80 cm, demonstrating the precision of the water level measurement by WS-TENG. In addition, a self-powered water level sensor based on a liquid-solid tubular triboelectric nanogenerator (LST-TENG) was designed for detecting ship draft [100]. Fig. 5e shows that LST-TENG is placed on the bow of a LNG (Liquefied Natural Gas) ship, which can help the crew to get the real-time ship draft without leaving the cabin. As shown in Fig. 5f, the LST-TENG consists of a main individual copper electrode and several other copper electrodes uniformly distributed along a PTFE tube. Seawater will enter the tube periodically with the wave fluctuations, so that the water and PTFE tube produce alternating contact and separation, leading to the transfer of electrons between the top and the bottom electrodes. Fig. 5g shows experimental diagram of LST-TENG installed on a ship model in a water tank. When the water level stabilizes at a specific position, the dV_{OC}/dt value is almost constant zero, and it changes in a stepped manner during the loading and unloading of cargo (Fig. 5h), thus the water level is detected. The LST-TENG has a accuracy of 10 mm, which is ten times higher than the accuracy of conventional measurement techniques. An et al. [186] designed a block-inserting mechatronics panel to monitor the water level information in real time under harsh working conditions and realize the water level monitoring of the ship system in real-time.

In addition to the solid-liquid contact mode, the output effect of solid-solid contact mode will be more significant. Zhang et al. reported a self-powered triboelectric ocean wave height sensor (TOSS), which is adaptable to measure ocean surface waves in any directions [140]. The schematic diagram of the application of TOSS on an offshore drilling platform is shown in Fig. 5i. TOSS consists mainly of tubular triboelectric nanogenerator and hollow-ball foam buoy (HFB). The working principle of the TOSS is shown in Fig. 5j. When the HFB floats with the waves, the PTFE layer and external copper will alternately contact and separate, thus generating a current. Fig. 5k illustrates the performance of TOSS in detecting wave height. When the ocean wave heights are ranging from 2 to 12 cm, the corresponding transferred charges of TOSS increase linearly from 25 nC to 160 nC. TOSS can monitor the marine parameters around the platform to guarantee the safety of the platform work. Xu and Liang et al. [188,189] also applied liquid-solid contact and buoy structure to achieve wireless self-powered liquid level sensing with excellent stability, excellent linearity and high sensitivity. Moreover, Wang et al. [56] introduced an innovative magnetic field assisted non-contact and liquid-liquid interacting TENG using a new tribo-materials(ferrofluid), which effectively solves the problem of possible stains on the triboelectric interface and ensures reliable

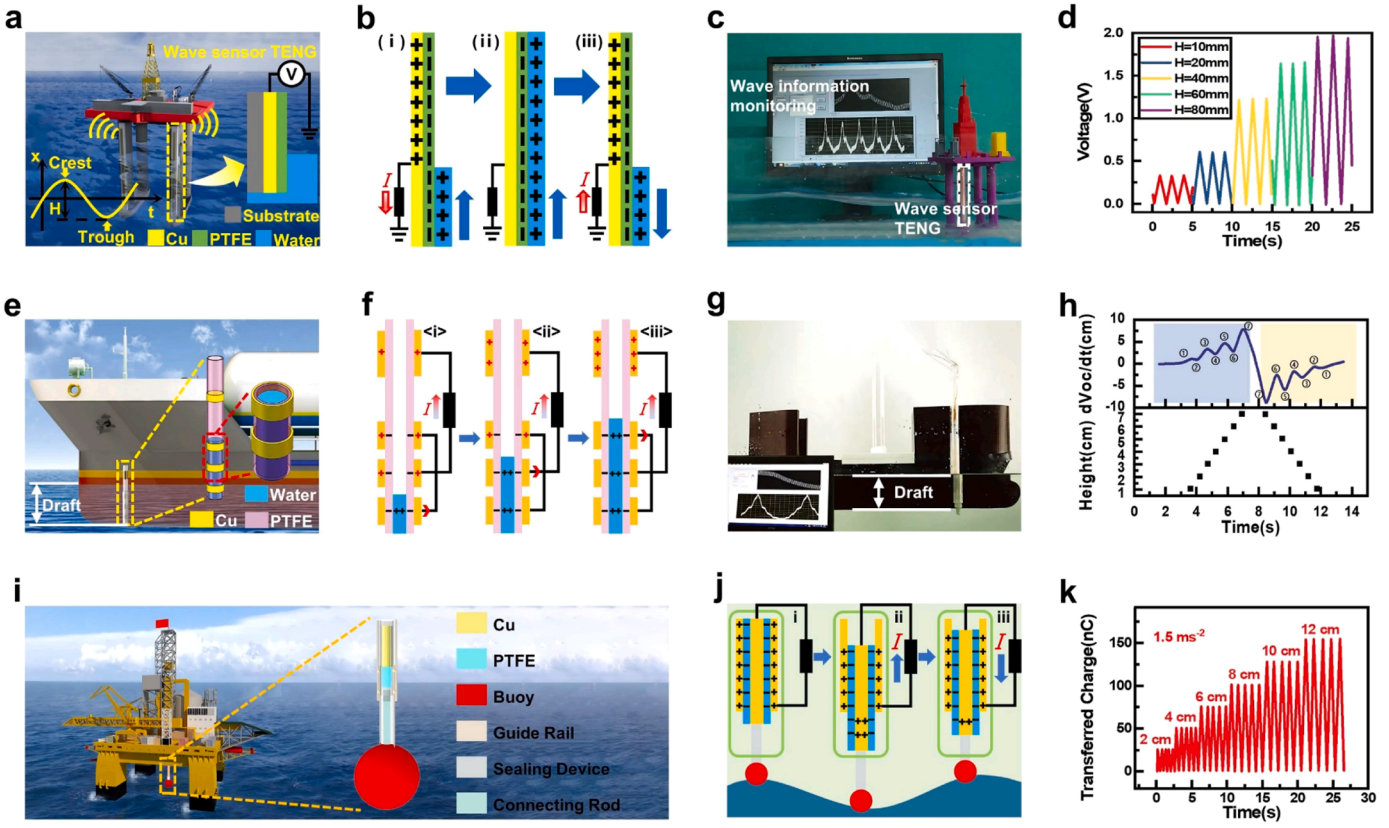

Fig. 5. The triboelectric displacement sensor: liquid level sensor. (a) Application diagram of WS-TENG on a marine platform. (b) The structure and principle of WS-TENG. (c) Schematic diagram of the test of WS-TENG in a water tank. (d) Output voltage of WS-TENG when the level height changes from 10 mm to 80 mm. Reproduced with permission from ref [187]. Copyright 2018 Elsevier. (e) Schematic diagram of LST-TENG. (f) Working principle of LST-TENG. (g) Experimental diagram of LST-TENG installed on a ship in a water tank. (h) The dV_{oc}/dt signals of LST-TENG and detected water level during the cargo loading and unloading of the ship. Reproduced with permission from ref [100]. Copyright 2019 Wiley-VCH. (i) Structural diagram of TOSS. (j) Working mechanism of TOSS. (k) Transferred charges of TOSS as a function of level height. Reproduced with permission from ref [140]. Copyright 2020 American Chemical Society.

operation under harsh working conditions.

3.2.2. Tilt angle sensor

Due to the high wind and wave climate at sea, ships and offshore structures generally appear to be in a state of sway, and monitoring of all tilt angles of sway is extremely necessary to prevent them from rolling over accidents. The more common working methods are solid-liquid contact type and rotary disk type. Firstly, Wang et al. proposed a tilt sensor to monitor ship's attitude based on liquid-solid interfacing triboelectric nanogenerator (S-TENG) [99]. With no moving parts and independence from the external environment, S-TENG offers advantages of outstanding durability and resistance to moisture, which provides a new option for intelligent ships. As is shown in Fig. 6a, S-TENG is made up of a circular PTFE tube with many copper electrodes uniformly aligned and some water in it. By simply fixing S-TENG to the ship's axis position, the real-time ship tilt angle can be monitored (Fig. 6b). More importantly, there is no significant difference between the results of S-TENG and those of commercial measuring instruments, as depicted in Fig. 6c, which illustrates the practical significance of the S-TENG in enhancing the automation and intelligence of ships. He et al. [184] also reporteded a Radial-Grating Pendulum-Structured Triboelectric Nanogenerator for Tilting-Angle Sensing using the characteristics of the pendulum structure, which has high sensitivity in terms of tilt angle and can easily perceive an angle change of more than 0.25°.

In addition to the above solid-liquid contact circular Angle sensor, the research of rotating disk is also getting more and more attention. Wu et al. reported a self-powered triboelectric multifunctional motion sensor (MFMS), which exhibits the capacity to detect the direction of both linear and rotational motions [106]. The structure of the MFMS is demonstrated in Fig. 6d. The MFMS is composed of an acrylic shell, a TENG module, and a magnetic regulation module. The TENG module consists of a free-standing magnetic disk (MD) and a PTFE plate with six copper electrodes. As schematically displayed in Fig. 6e, the MFMS movement drives MD to slide on the PTFE plate, generating a voltage output between the electrodes. Fig. 6f demonstrates the simulated output voltage waveform when the MD rotates clockwise on the PTFE plate. In a certain period of time, the East-E, South-E, West-E,North-E reach the maximum output performance to determine the rotation speed and direction. Similarly, Fang et al. [190] proposed a self-powered rotating mode tilt sensor thriving on soft contact and can output an open circuit voltage of ~12 V even when the tilt angle is 1° at ultra-low speed. Moreover, Wu et al. introduced a quasi-static triboelectric sensor (QS-TES) for angle detection from rotational motion [141]. Fig. 6g exhibits the structure of the QS-TES. It is made up of two parts, a rotor coated with a four-channel coded copper foil and a stator coated with a vinyl fluoride propylene film. Fig. 6h illustrates the principle of angle measurement. The sensor responds to the mechanical rotation of the object mounted with the sensor. When the output voltage of each channel reaches positive peak, it represents alignment between the copper foil sector and the bottom electrode. On the contrary, it represents alignment between the carved sector and the bottom electrode. By analyzing the output signals from the four channels, it is possible to determine the position of the rotator and subsequently calculate its angular displacement. As shown in Fig. 6i, the output voltages from the four channels are logged and promptly displayed via indicators on a computer monitor when a steering wheel undergoes one full

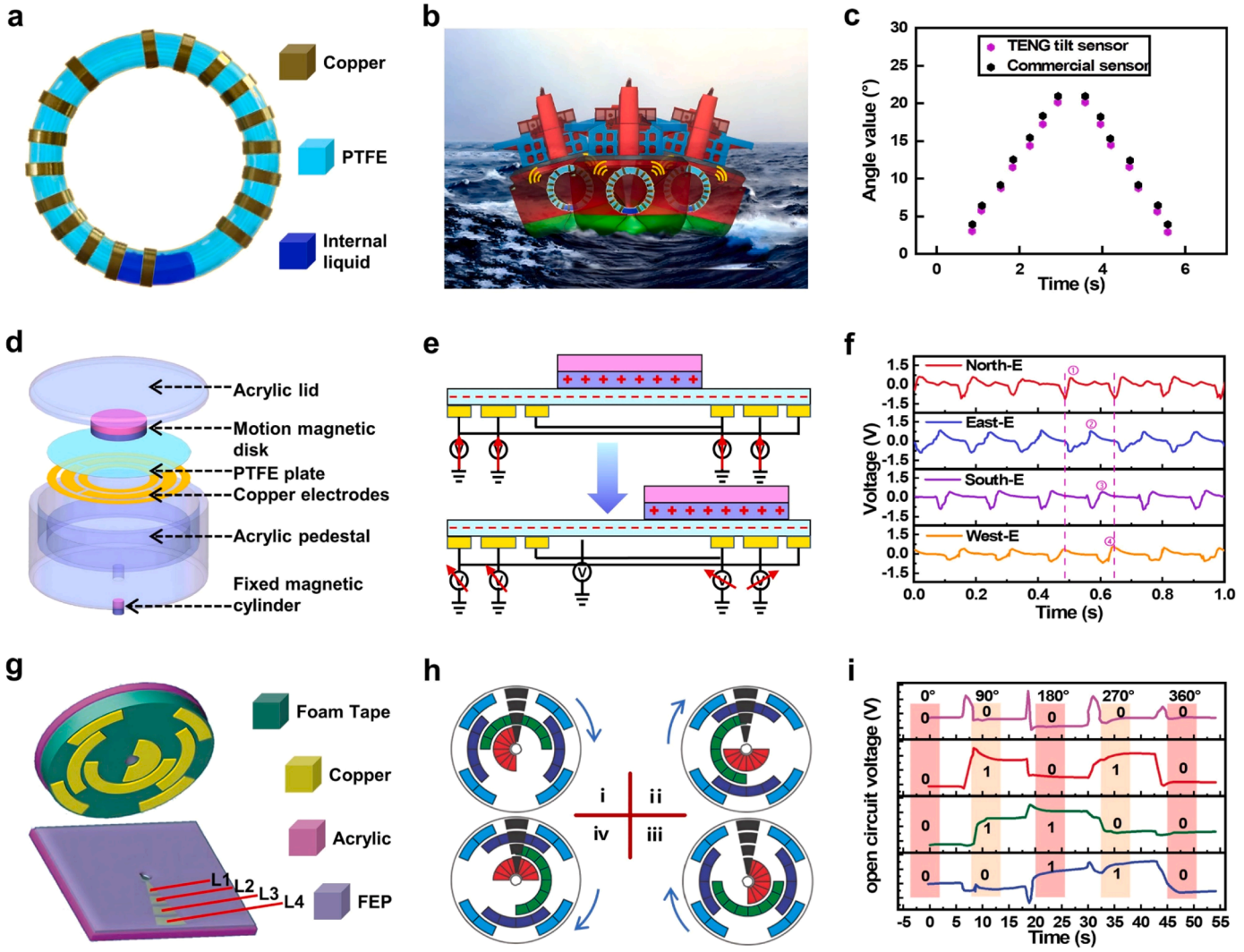

Fig. 6. The triboelectric displacement sensor: tilt angle sensor. (a) Structural design and working principle of the TENG tilt sensor. (b) Application of the TENG tilt sensor for monitoring the heel of a ship. (c) Comparison of the Angle value measurement between TENG tilt sensor and commercial sensor. Reproduced with permission from ref [99]. Copyright 2020 Elsevier. (d) Structural diagram of MFMS. (e) Working mechanism of MFMS. (f) Relationship between voltage waveforms of four arc electrodes and moving direction of MD. Reproduced with permission from ref [106]. Copyright 2018 American Chemical Society. (g) Schematic diagram of QS-TES. (h) Working mechanism of QS-TES. (i) Open-circuit voltage and codes of output signal under various rotation angles. Reproduced with permission from ref [141]. Copyright 2015 Wiley-VCH.

counterclockwise rotation. Hou et al. [183] also designed a special bi-directional backstop rotation structure based on the angle vector sensor, which can realize separate measurement of angle changes in each direction, and provides a new strategy for TENG in the field of angle measurement.

In general, the triboelectric displacement sensor shows unique advantages over traditional liquid level sensors in detecting ship draft and wave height. Based on the working modes of liquid-solid contact and solid-solid contact, it achieves stable, high-sensitivity and high-precision liquid level sensing. In addition, the development of new triboelectric materials also promotes the development of non-contact mode and liquid-liquid mode, which greatly improves the adaptability to harsh working conditions. Through the fusion of triboelectric displacement sensor and other kinds of sensors, the high-precision perception of multi-dimensional information of ship and marine environment can be realized, which provides data support for the optimal design and management of ship and marine engineering. Through digital twin technology, the virtual model of ship and marine environment can be established, and the real-time monitoring and prediction of ship draft and wave height can be realized, which provides decision support for the operation and maintenance of ship and marine engineering. The fusion of triboelectric tilt angle sensor and artificial intelligence is also an effective method to improve the accuracy and robustness of the sensing system. Through machine learning technology, a large number of electrical signals generated by the triboelectric tilt angle sensor can be processed and intelligently identified to achieve high-precision attitude estimation, improve the accuracy, stability and reliability of the sensor, and reduce the influence of temperature, humidity and electromagnetic interference. Advanced machine learning algorithms such as DL and neural networks can be combined to improve their integration with artificial intelligence to achieve more complex perceptual tasks. In the future, we will continue to explore the potential of the fusion of triboelectric tilt angle sensor and artificial intelligence in MIoT applications such as intelligent ships and marine structure monitoring.

3.3. *Triboelectric flow sensor*

The triboelectric flow sensor has made a great contribution to the flow monitoring. It could monitor the flow of fluid without an external power source in the pipeline of ships or offshore platforms [191–193].

When the fluid flows, there is alternating contact and separation between the different tribo-materials inside the sensor, which converts the mechanical movement of the fluid into an electrical signal. Since various fluids have different mechanical motion properties, the triboelectric flow sensors are also different in structural design and material selection. According to different detection targets, the triboelectric flow sensors are mainly divided into two categories: triboelectric single-phase flow sensors and triboelectric multiphase flow sensors.

3.3.1. *Single-phase flow rate sensor*

Single-phase flow rate sensors are the most common application on ships, and they are used for gas and liquid transportation in general pipelines. Among the more common structures are thin film flapping type and rotating turbine type. First of all, Chen et al. proposed a low pressure loss gas flowmeter utilizing a membrane's flutter driven triboelectric nanogenerator (TENG flowmeter) for monitoring the flow in a pipeline [142]. Fig. 7a depicts a physical view of the three TENG flowmeters being used for fluid monitoring in the pipelines. The TENG flowmeter is installed in the middle of the pipe, and the flow rate can be obtained from the upper display as air passes through. Since TENG flowmeter is well sealed, it does not cause significant pressure loss in the piping system. Fig. 7b shows the structure of the TENG flowmeter, which consists of a polyvinyl chloride (PVC) pipe, two copper electrodes and a thin film. When a sufficiently high velocity airflow flows through the pipe, the airflow causes the film to vibrate and make contact with the upper and lower copper electrodes, generating an alternating current signal. Fig. 7c shows the correlation between the flow rate and the vibration frequency. Regardless of the length of the diaphragm, there is a clear linear relationship between the gas flow rate and the vibration frequency, so the measurement accuracy of the TENG flowmeter is very high.

For rotating turbine type, Chen et al. proposed a bladeless turbine-based triboelectric nanogenerator (BT-TENG), which is integrated within a fluidic system as a self-powered flow rate sensor [143]. Fig. 7d dipicts a structural diagram of BT-TENG, which is composed of the bladeless turbine and a rotational TENG. BT-TENG can transform the fluid flow into rotational motion, which drives the rotational TENG. Fig. 7e shows the working principle of BT-TENG. When the working fluid is blown in, the turbine rotates to create alternating contact and separation between the PTFE and the two electrodes, resulting in charge transfer. As shown in Fig. 7f, there is a good linear relationship between flow rate and output current. When the output current of the BT-TENG

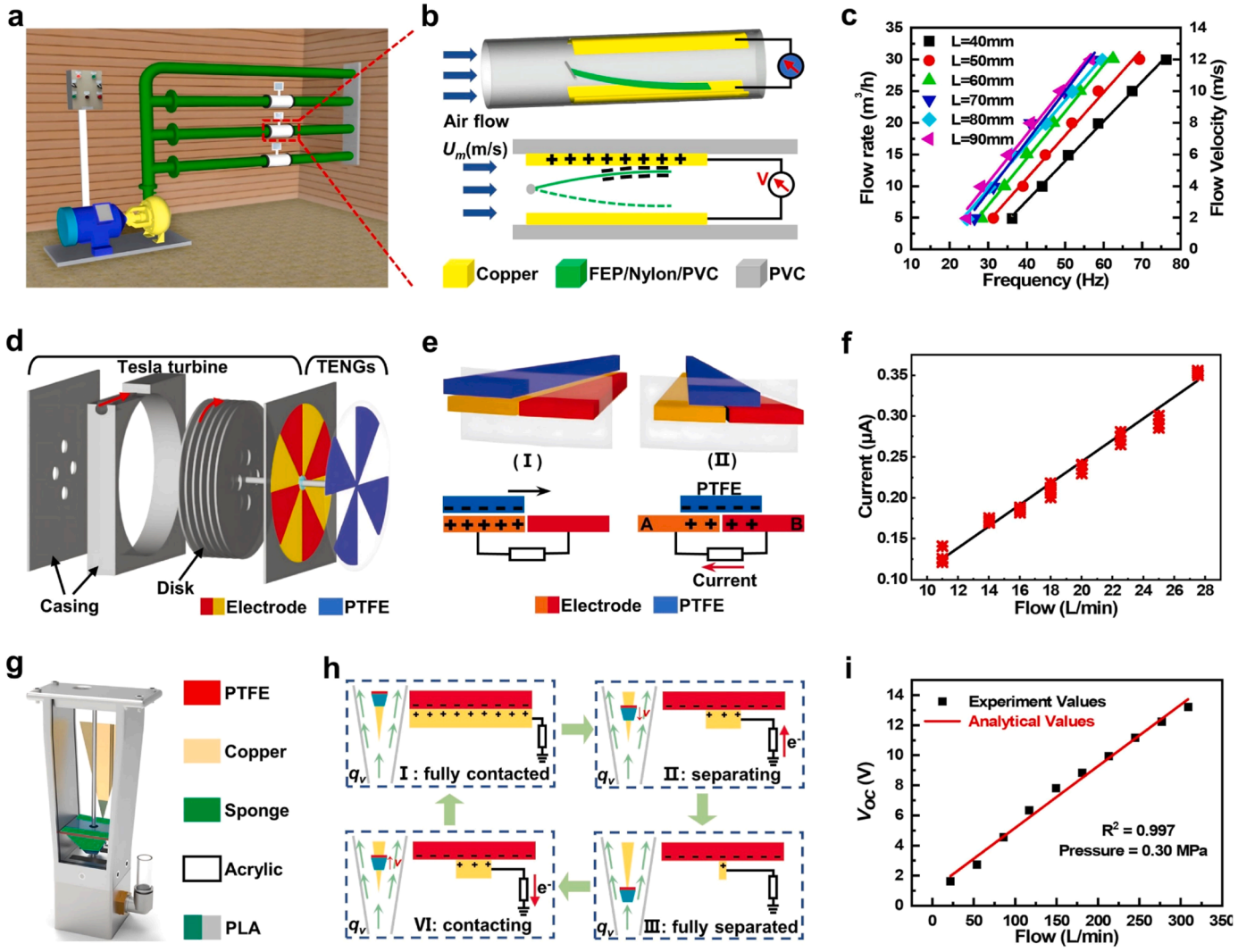

Fig. 7. The triboelectric flow sensor: single-phase flow rate sensor. (a) Applicational diagram of FE-TENG in pipeline. (b) Structural diagram and working principle of FE-TENG. (c) Pipe flow rate and flow velocity versus the vibration frequency. Reproduced with permission from ref [142]. Copyright 2020 MDPI. (d) Schematic diagram of BT-TENG. (e) Working mechanism of BT-TENG. (f) Linear relationship diagram of current signal and flow. Reproduced with permission from ref [143]. Copyright 2019 Wiley-VCH. (g) Structural design of TFS with float-cone structure. (h) Working principle of TFS. (i) Dependence of open voltage the TFS on the flow. Reproduced with permission from ref [109]. Copyright 2019 Wiley-VCH.

increases from 0.125 V to 0.35 V, the flow rate gradually increases from 11 L/min to 28 L/min. Wang et al. [193] also engineered a water-liquid-driven rotating triboelectric nanogenerator that can be mounted in any waterway system using a water meter structure. As a smart water meter, it can monitor water flow in real time and can perform electrostatic anti-scaling and anti-rust. Du et al. [191] proposed a marine exhaust gas flow sensor with a new type of turbine bearing structure suitable for harsh working conditions and the average error is about 0.73% compared with the commercial gas flow sensor. In addition, Wang et al. designed a triboelectric flow sensor (TFS) with a float-cone structure for flow monitoring [109]. Fig. 7g shows the detailed structure of TFS, which is made up of an outer translucent conical shell and an inner float. Fig. 7h illustrates the working principle of TFS. In the starting state, the float is at its lowest position. As the air flow alters, the buoy oscillates vertically along the electrode and a current signal will generate between the electrode and the ground. As shown in Fig. 7i, the linear correlation coefficient between the flow rate and the open circuit voltage is 0.997, which characterizes the good performance of TFS for gas flow detection. By introducing an internal floating system, TFS offers better measurement accuracy and flexibility, providing a new option for industrial flow monitoring. On this basis, Wang et al. [111] developed a magnetic flap type difunctional sensor for pneumatic flow and liquid level detection, which can effectively detect the fluid surface elevation of 30-130 mm. Cheng and Wang et al. [194, 195] also applied film flapping type and rotating turbine type to achieve single-phase flow rate sensing.

3.3.2. *Multiphase flow rate sensor*

Multiphase flow generally refers to two-phase flow and above. Two-phase flow system is extensively utilized in the industrial field. Two-phase flow detection is especially critical in pneumatic pipes, and TENG provides a new way for detecting two-phase flow systems. At present, the research focus of two-phase flow mainly focuses on the gas-solid and gas-liquid modes. For gas-solid mode, Wang et al. developed a triboelectric gas–solid two-phase flow sensor (GS-TENG), which measures the mass flow and the particle concentration in a two-phase pipeline [144]. Fig. 8a shows the application scenarios of the GS-TENG in a pipeline system. When the industrial material flows into

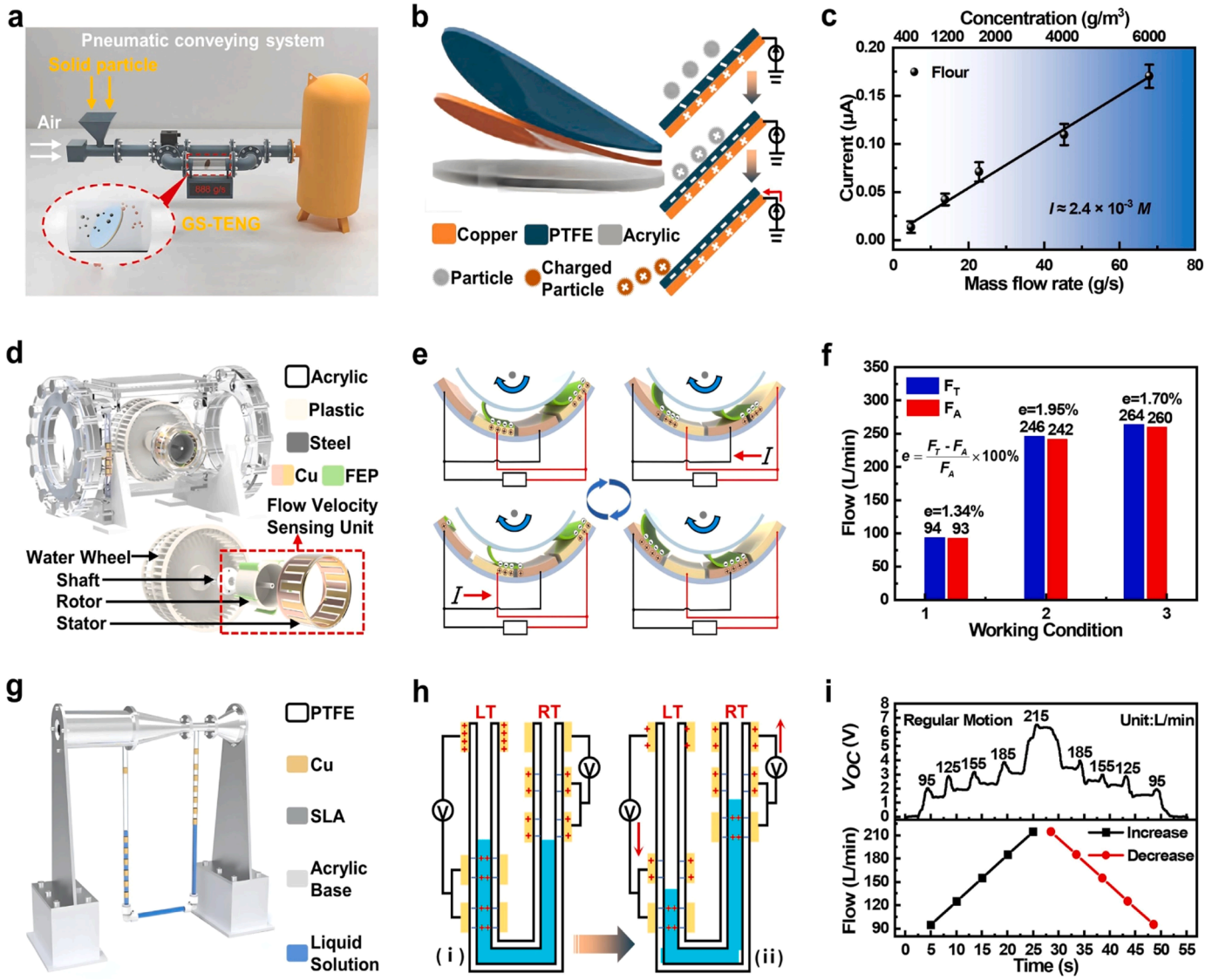

Fig. 8. The triboelectric flow sensor: multiphase flow rate sensor. (a) Application drawing of GS-TENG. (b) Working principle of GS-TENG. (c) Relationship between the current signal and the different mass flow rate. Reproduced with permission from ref [144]. Copyright 2021 Wiley-VCH. (d) Structural graph of TNPFS. (e) Working mechanism of TNPFS. (f) Comparison of the TNPFS and actual measured flow under various working condition. Reproduced with permission from ref [108]. Copyright 2022 American Chemical Society. (g) Structural diagram of VTTFS. (h) Working principle of VTTFS. (i) Curve of open-circuit voltage signal obtained when the flow changes regularly. Reproduced with permission from ref [124]. Copyright 2021 Elsevier.

the pneumatic conveying system, the valve on the branch pipeline is opened for continuous sampling and testing during the contact between the industrial material and the GS-TENG surface. Fig. 8b illustrates the structure and working principle of GS-TENG, which consists of three parts: one PTFE film, one copper electrode, and one acrylic plate. Alternating contact and separation of the particles with the PTFE surface of the sensor causes an electric current to be generated between the copper electrode and the ground. Fig. 8c shows a good linearity between the mass flow rate of the flour and the peak output current of GS-TENG. In addition, the GS-TENG indicates high sensitivity and high precision-with the error less than 2.0%. The GS-TENG can be employed for real-time monitoring and pre-warning of mass flow in industrial gas delivery systems. Xu et al. [196] also designed a new type of gas-solid two-phase flow sensor working on a single electrode mode, which can be used as a solid transport rate sensor according to the output current. Beyond that, Gu and Wang et al. [197,198] have made some explorations on solid particle transport and particle identification in pipelines, and have made some achievements in mass flow monitoring, particle identification, and equipment fault diagnosis.

For gas-liquid mode, He first et al. reported a triboelectric non-full pipe flow sensor (TNPFS) to accurately monitor flow rate for large pipelines [108]. Fig. 8d exhibits the overall structure of TNPFS. It is composed of a transparent acrylic cylinder, a water wheel rotating structure, a liquid level sensing unit and a flow rate sensing unit. Fig. 8e illustrates the working mechanism of the TNPFS. When the fluid in the pipe drives the rotor to rotate, the flexible FEP blades slide between the two copper electrodes, creating an alternating current signal. Fig. 8f shows that the measured value of TNPFS is very close to the actual measured flow rate, with an error rate of less than 1.95%. TNPFS offers an innovative method for fluid flow monitoring, particularly the non-full pipe flow of large pipelines. Moreover, Wang et al. proposed a Venturi-type triboelectric flow sensor (VTTFS) based on a liquid-solid contact-electrification waveform coupling method [124]. As demonstrated in Fig. 8g, the VTTFS is mainly comprised of a commercial PTFE U-tube, a Venturi tube, and a support frame. Fig. 8h illustrates the working mechanism of VTTFS. As the fluid solution in the PTFE U-tube is driven by the pressure difference in a tube, the triboelectric effect will cause the liquid solution to have a net positive charge, while the surface of the PTFE U-tube has an equal density of net negative charge. As the flow rate changes through the Venturi tube, a pressure difference occurs and a current signal will be generated between the electrodes owing to electrostatic induction. Effective and accurate flow detection is achieved by counting and identifying the pulses generated by VTTFS. Fig. 8i shows the variation of the output voltage of the VTTFS when the flow rate changes regularly, indicating that the corresponding number of pulses has a good linearity with the increase and decrease of flow rate. In addition, Zhang et al. [192] reported a bubble motion-based triboelectric sensor, which can be used not only to detect the water flow rate in pipeline, but also to detect blockage and leakage in the fluid pipe with an accuracy of 10 cm.

To sum up, there are two types of triboelectric single-phase flow rate sensors: film flapping and rotating turbine. The film flutter sensor uses the impact force of fluid on the film to generate a triboelectric signal. A rotating turbine sensor uses a fluid to push the turbine, causing it to spin and generating a triboelectric signal. The single-phase flow rate sensor can be used as a smart water meter, and can also use static electricity for anti-scaling and anti-rust treatment. In addition, the sensor has the characteristics of strong environmental adaptability, can automatically adjust parameters according to the temperature, pressure and viscosity of the fluid, and can also measure the liquid level and flow at the same time, which has great application prospects in the transport of gases and liquids on ships. Triboelectric multiphase flow rate sensors can be used for mass flow rate monitoring and non-full pipe flow rate monitoring of large pipelines. There are two main types of operation: gas-solid and gas-liquid mixed fluid flow. Gas-solid flow rate sensor can identify the type and amount of particles and can diagnose equipment faults. The gas-liquid flow rate sensor can be used for the non-uniform flow of gas-liquid, and can monitor the blockage and leakage in the pipeline. This sensor has the characteristics of high precision and can measure the instantaneous and cumulative flow of the fluid, as well as the phase distribution of the fluid. As a new technology, artificial intelligence can greatly improve the intelligence level of triboelectric flow rate sensor and realize the intelligent analysis and decision of fluid. Artificial intelligence imbues triboelectric flow rate sensors with intelligence and high adaptability, improving their ability to perceive and process complex fluid behavior through different learning and simulation techniques. This integration will make the triboelectric flow rate sensor more flexible and intelligent, which is expected to play a more important role in the monitoring and control of the fluid field.

3.4. Triboelectric vibration sensor

The triboelectric vibration sensor uses the vibration generated during the operation of mechanical equipment to drive the contact and separation between different tribo-materials and generate electrical signals, which can realize the perception of vibration signals such as amplitude [199–202], frequency [203–205], speed [206–208] and acceleration [209–211]. By monitoring the working status and marine environmental parameters of marine machinery equipment and systems, it realizes the functions of equipment status detection, fault diagnosis and optimization of working conditions. It plays a very important role in the entire marine sensor network. According to the different motion modes of the triboelectric vibration sensor, this paper mainly divides into two categories: harmonic triboelectric vibration sensor and non-harmonic triboelectric vibration sensor.

3.4.1. Harmonic vibration sensor

When the vibration sensor is excited by harmonic vibration, the moving parts inside the sensor will always move symmetrically on both sides of the equilibrium position. Recently, great efforts have been made in the development of triboelectric harmonic vibration sensors. Generally, springs and spring-assisted structures are used as core components to accompany the periodic reciprocating motion of the measured object, and the working state of the vibration system can be monitored through the electrical signals generated by them. Using the spring as the core component, Hu et al. designed an automatic suspended 3D-spiral structural vibration sensor (S-TENG) for acceleration detection [212]. The structure of the S-TENG is shown in Fig. 9a. which consists of a round aluminium (Al) plate attached to the 3D spiral structure and another round kapton plate fixed in the center of the upper surface of the cube's bottom. Fig. 9b depicts the working principle of the S-TENG. When the spiral oscillates due to external mechanical perturbations, the Al electrode and the kapton film alternately contact and separate to produce electrical signals. As shown in Fig. 9c, the output voltage signal increases linearly with the increase of vibration acceleration. Therefore, S-TENG can precisely determine vibration amplitude and vibration source location. On the basis of the spring-assisted structure, Qi et al. [213] used the paper-cut process to optimize the structure design, which is used as a vibration acceleration sensor with a measurement range from 1 to 9 m/s^2. In addition, Li et al. proposed a fully self-powered vibration sensing system driven by dual-mode triboelectric nanogenerator (AC/DC-TENG), which can satisfy the need of real-time monitoring of the vibration condition [145]. Fig. 9d shows the application scenario of AC/DC-TENG to monitor the vibration safety state of a bridge construction, and the enlarged image is the structure of AC/DC-TENG, which consists of a stator and a slider. Fig. 9e shows the working mechanism of AC/DC-TENG. When the slider slides in the safe zone, AC signal will be generated. When a part of the slider moves in the danger zone, a DC signal will be generated and trigger the alarm light immediately. As shown in Fig. 9f, the V_{AC} and V_{DC} presents a good linear relationship with vibration amplitude in the safe zone. Therefore, AC/DC-TENG can offer a convenient and effective method for

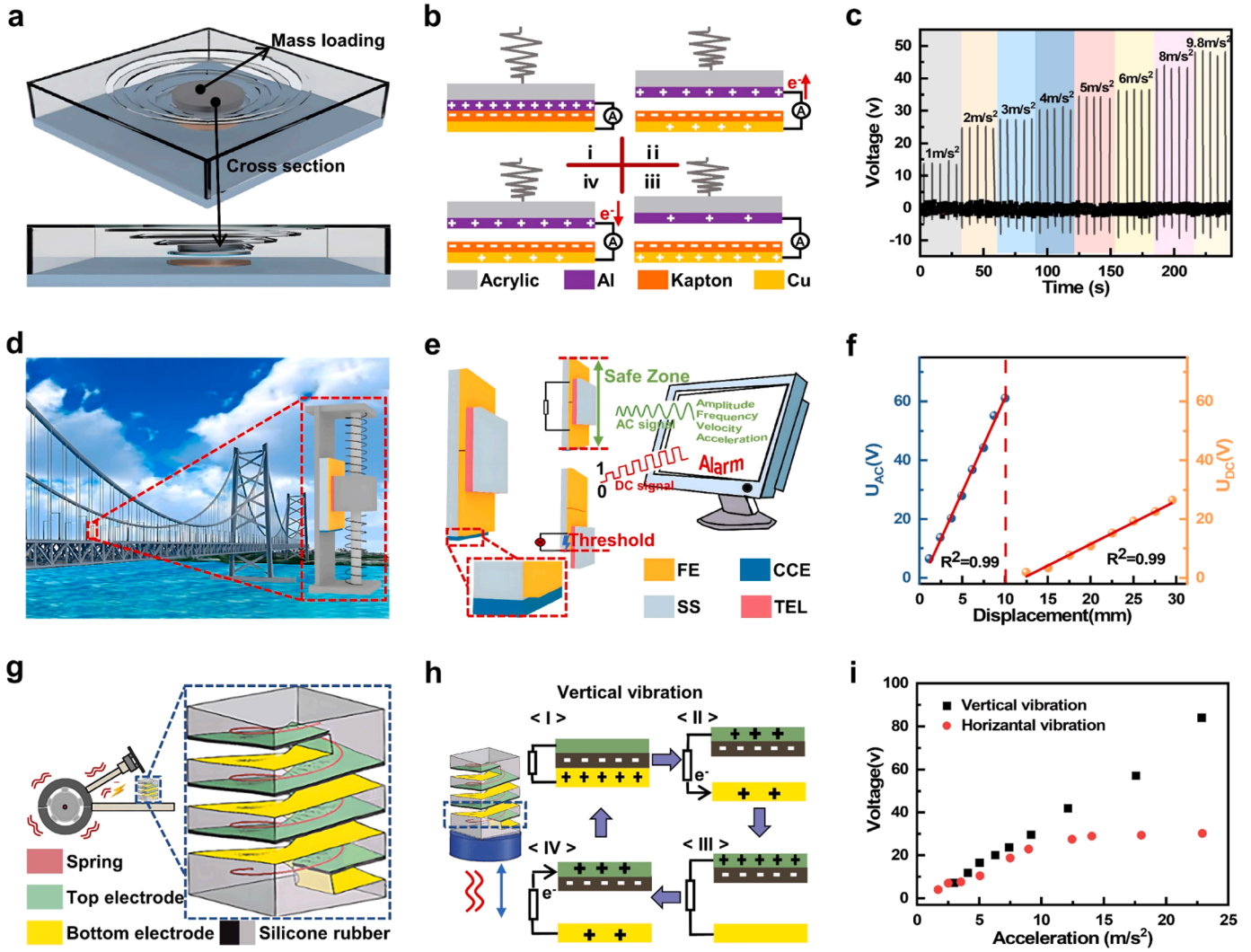

Fig. 9. The triboelectric vibration sensor: harmonic vibration sensor. (a) Structure of S-TENG. (b) Schematic diagram of working process of the S-TENG. (c) S-TENG output voltage when the acceleration changes from 1 to 9.8 m/s^2. Reproduced with permission from ref [212]. Copyright 2013 American Chemical Society. (d) Schematic structure of AC/DC-TENG. (e) The working mechanism of AC/DC TENG. (f) AC/DC TENG in VAC and VDC at different displacements. Reproduced with permission from ref [145]. Copyright 2020 American Chemical Society. (g) Diagram of the spiral structure of S-TENG. (h) Working mechanism of the S-TENG. (i) Relationship between average peak voltage and acceleration under vertical excitation of S-TENG. Reproduced with permission from ref [146]. Copyright 2017 Wiley-VCH.

monitoring the vibration amplitude and health status of marine construction structure. By reducing the size and improving the shape of the structure, Mehamud et al. [128] made a spring-assisted vibration sensor that can detect major mechanical faults and defects in a wide range of 0 ~ 1200 Hz.

Using the spring-assisted structure as the core component, Xu et al. designed a soft spring based triboelectric nanogenerator (S-TENG) for self-powered vibration acceleration and frequency sensing [146]. As illustrated in Fig. 9g, the S-TENG is composed of silicone rubber, spring and a conductive elastomer electrode, forming a helical structure along a spring wire. Fig. 9h exhibits the working principle of the S-TENG. The periodic contact and separation between the silicone rubber and the top electrode can generate electrical signals. When the S-TENG is excited vertically, the output voltage signal increases linearly with the vibration acceleration, and the range of 0 m/s^2 ~ 25 m/s^2 can be detected (Fig. 9i). Under horizontal vibration excitation, the output performance deteriorates due to insufficient contact between dielectric materials. Therefore, it can better present the sensing advantages when used as a vertical vibration sensor, showing great application potential in the vibration state monitoring of ship machinery. Ren et al. [214] proposed a trapezoidal cantilever structure triboelectric nanogenerator, which can effectively sense the low-frequency vibration of the environment. Beyond that, Liu et al. [209] proposed a vibration sensor with a high sensitivity of 20.4 V/(m/s^2).

3.4.2. *Non-harmonic vibration sensor*

When the vibration sensor is excited by non-harmonic vibration, it will not show sine-wave vibration, but reciprocating on both sides of the equilibrium position. The moving parts inside the sensor are no longer limited by core components such as springs, and can move freely with the measured object. At present, the two tribo-materials inside the vibration sensor are mainly plane contact and spherical contact. For plane contact mode, Du et al. developed a silicon rubber strip-based triboelectric nanogenerator (SRS-TENG) for self-powered sensing vibration frequency, amplitude and acceleration [147]. As shown in Fig. 10a, SRS-TENG can be employed as a vibration sensor for various applications on the ships. Fig. 10b depicts the structure of SRS-TENG, which mainly consists of two conductive Al electrodes and a non-conductive silicone rubber strip. As shown in Fig. 10c, the silicone rubber strip produces oscillating elastic deformation due to external excitation, and

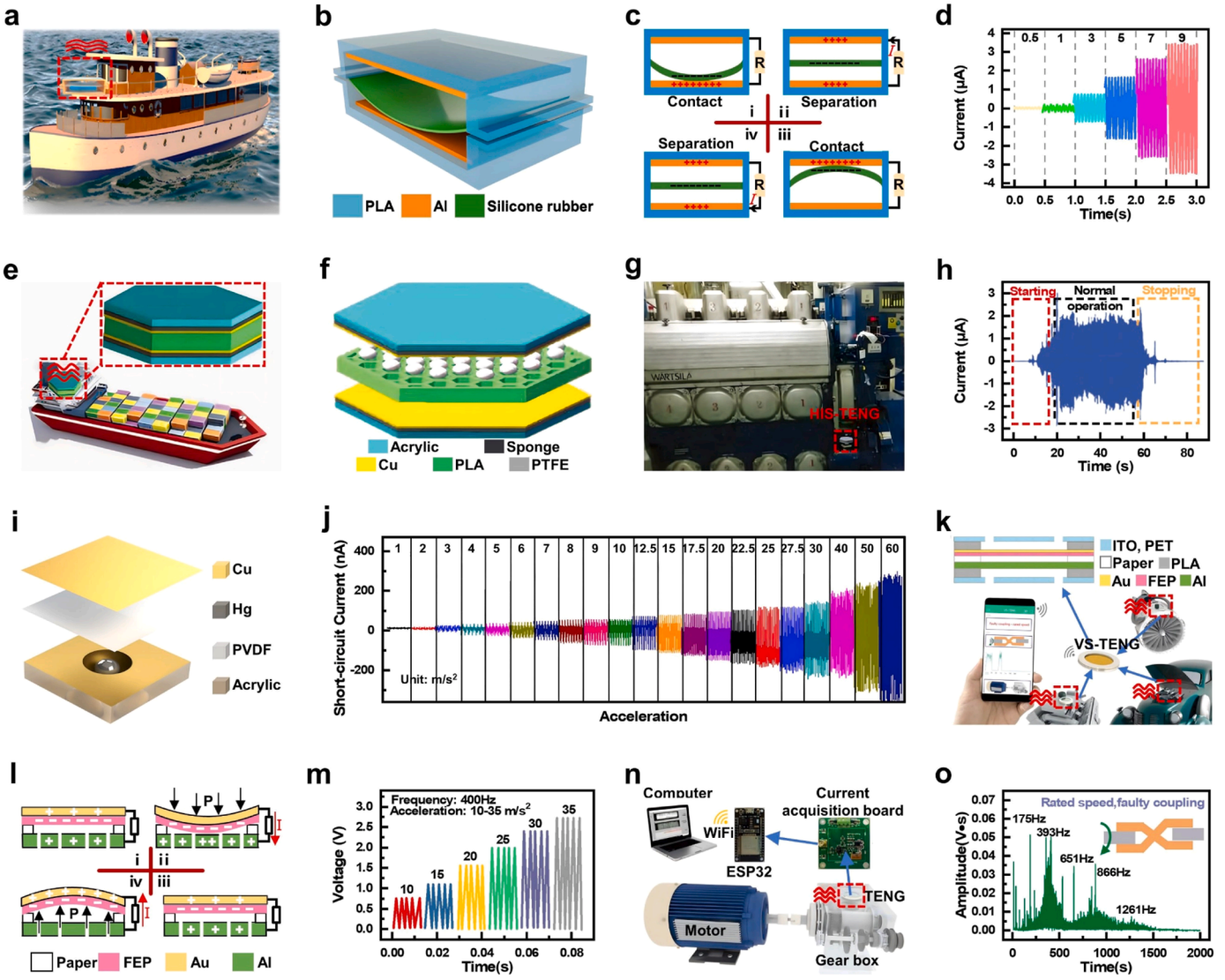

Fig. 10. The triboelectric vibration sensor: non-harmonic vibration sensor. (a) Application scenarios of SRS-TENG. (b) Schematic structure of the SRS-TENG structure. (c) Working mechanism of SRS-TENG. (d) Dependence of the output current of the SRS-TENG on the amplitude. Reproduced with permission from ref [147]. Copyright 2022 MDPI. (e) HSI-TENG for vibration sensing. (f) Structure of the HSI-TENG. (g) Photograph of HSI-TENG for diesel engine monitoring. (h) Short-circuit current of HSI-TENG in different operating conditions. Reproduced with permission from ref [11]. Copyright 2019 Wiley-VCH. (i) Structural design of the LM-T. (j) Curve of short-circuit current with acceleration for LM-T. Reproduced with permission from ref [14]. Copyright 2017 American Chemical Society. (k) VS-TENG application scenarios and structure. (l) Power generation cycle of VS-TENG (m) VS-TENG open-circuit voltage at accelerations of 10 to 35 m/s^2. (n) Schematic diagram of mechanical condition monitoring by VS-TENG. (o) Spectrogram of gearbox in case of coupling failure. Reproduced with permission from ref [103]. Copyright 2022 Wiley-VCH.

alternately contacts and separates the two Al electrodes to generate electrical signals. As illustrated in Fig. 10d, the output short-circuit current of the SRS-TENG increases linearly with the vibration amplitude at a fixed vibration frequency. Therefore, SRS-TENG has potential application prospects in self-powered vibration sensing in the field of ship and ocean engineering. Zhang et al. [215] proposed a magnetic levitation triboelectric nanogenerator, which can clearly detect vibration acceleration less than 30ms^{-2} and amplitude less than 7.5 mm.

For spherical contact mode, Xiao et al. first reported a honeycomb structure-inspired triboelectric nanogenerator (HSI-TENG), which offers a new paradigm for mechanical vibration monitoring [11]. Fig. 10e exhibits the application of the HIS-TENG, which is installed on the ship to monitor the working condition of the diesel engine in real time. Fig. 10f shows the structure of the HSI-TENG, which is made up of one honeycomb frame and two copper electrode layers with sponge bases. When the HSI-TENG vibrates with the mechanical operation (Fig. 10g), the PTFE balls inside the frame move upward and downward, and contact and separate with the upper and lower copper electrode films alternately to generate electrical signals. Fig. 10h shows the output current of HSI-TENG during the starting, normal operation and stopping of the diesel engine. Zhang et al. reported a self-powered and highly sensitive acceleration sensor based on liquid metal (LM-TENG) with a detection range from 0 to 60 m/s^2 and a sensitivity of up to 0.26 V·s/m^2 [14]. Fig. 10i schematically shows the structure of LM-TENG. It is composed of a Hg droplet and nanofiber-networked polyvinylidene fluoride (nn-PVDF) film. There is also a hemispherical pit with a diameter of 10 mm cut out of the surface of an acrylic plate, coated with a thin copper film to serve as a movement space for mercury droplets, and the top of the pit is sealed by nn-PVDF. Fig. 10j shows the short-circuit current of the sensor under different accelerations, presenting the application prospect of LM-TENG in vibration monitoring and troubleshooting of equipment. To further increase the contact area, Zhao et al.

developed a highly sensitive triboelectric vibration sensor (VS-TENG) [103]. The application scenario of the VS-TENG is shown in Fig. 10k. The output signal of VS-TENG can be transmitted to the server through the wireless network and can be displayed on a computer or handheld mobile device. Fig. 10l demonstrates the working principle of VS-TENG. When externally excited by a vibration source, the alternating contact and separation between the FEP film and the aluminum foam produces a current. Fig. 10m illustrates the open-circuit voltage signals of VS-TENG under different accelerations at a fixed frequency, showing a good linear relationship. Fig. 10n shows the schematic diagram of VS-TENG mechanical condition monitoring. The spectrogram of the gear box in the case of coupling failure, as shown in Fig. 10o, shows that the VS-TENG has been successfully used for monitoring the operating condition of mechanical gear systems, as well as vibration monitoring of infrastructure in industry. Lin and Guo et al. [49,216] also further optimized the design on the basis of spherical contact and the accuracy can reach more than 95%. In addtion, Gao et al. [199] proposed a self-powered multifunctional vibration sensor, which provides an effective method for vibration monitoring, especially in extreme environments or unattended situations.

In general, the triboelectric vibration sensor plays a key role in the MIoT, and realizes the functions of equipment condition detection, fault diagnosis and working condition optimization by monitoring the working state of marine equipment and systems. The harmonic triboelectric vibration sensor is mainly based on spring and spring auxiliary structure to realize the perception of vibration frequency and amplitude, which provides a convenient and effective method for the health monitoring of marine building structures and equipment. Non-harmonic triboelectric vibration sensor, which relies on the plane contact and spherical contact mode of two triboelectric materials, provides a new model for real-time vibration monitoring of marine machinery and marine engineering health assessment. The development of new structures such as the liquid-solid TENG has greatly improved the sensitivity and detection range. At the same time, it can be transmitted to the server through a wireless network and can be displayed on a computer or handheld mobile device to achieve data visualization. The introduction of artificial intelligence can more accurately extract the frequency, amplitude, phase and other information of vibration. Through machine learning technology, the electrical signal can be filtered, noise reduction, feature extraction, pattern recognition and other processing, so as to realize the intelligent recognition of vibration source, vibration type, vibration state, etc., and improve the accuracy, stability and reliability of the sensor. Artificial intelligence can also further analyze and model the data through DL, neural network and other technologies, so as to realize the prediction and control of vibration, and provide decision support for the operation and maintenance of equipment. In addition, through machine learning, digital twin and other methods, the data of different sensors are fused and optimized, complementary iteration, so as to improve the perceptual accuracy and working stability.

3.5. Triboelectric velocity sensor

Triboelectric velocity sensor is a kind of velocity sensing sensor that does not require external energy supply. It can generate electrical signals from friction or contact-separation between different tribo-materials by absorbing kinetic energy in the moving system to realize velocity information sensing. In the field of marine engineering, it is mainly used to perceive the rotation speed of mechanical equipment [217–221] and the flow speed of fluid in the marine environment [115,195,222,223], so as to timely feedback the operating status of mechanical equipment, enrich the flow field information, and improve the transparency of the marine environment [224–228]. According to the different structure, the triboelectric velocity sensor is divided into two categories: triboelectric mechanical rotational speed sensor and triboelectric fluid velocity sensor.

3.5.1. Mechanical rotational speed sensor

When themechanical rotational speed sensor measures the speed of the mechanical equipment, the moving parts of the sensor will also rotate with the rotating shaft of the machine being measured, so that it will alternately contact and separate with its stationary parts, thus generating electrical signals. The common working mode mainly adopts the freestanding triboelectric-layer mode, and the tribo-material generally adopts the spherical contact and the plane contact mode. For spherical contact mode, Xin et al. introduced a ring-type triboelectric nanogenerator (R-TENG) a self-powered rotational speed sensor of the rotating machinery [229]. The potential application scenarios of the R-TENG is shown in Fig. 11a. Fig. 11b depicts the schematic structure of the R-TENG mounted on the rotating shaft. The R-TENG is made up of a container unit mounted a PTFE cylinder, an end cover and a pair of aluminum strips parallelly coated to the inner and outer walls of the workspace. Fig. 11c presents the working principle of the R-TENG. As the R-TENG continues to rotate with the shaft, a potential difference is formed between the two electrodes to generate alternating current in the external circuit due to the relative motion between PTFE cylinder and electrode. Fig. 11d shows the current signals at different rotational speed. With the increase of the rotational speed, the current I_{sc} increases steadily. Han et al. [230] also proposed a intelligent rolling bearing based on spherical contact mode, and the current has a linear relationship with the rotational speed in a wide range.

For plane contact mode, a self-powered triboelectric smart roller-bearing was proposed for measuring rotational movement [148]. The electrical signals generated by the smart bearing enables continuous monitoring of the rotational speed and the operating conditions of the components. A schematic diagram of the completed assembly of all component parts is shown in Fig. 11e. The detailed components of the triboelectric sensor are depicted in Fig. 11f. The triboelectric sensor mainly consists of an inner ring, an outer ring, several rollers, and the electrodes. The inner and outer bearing rings and the 12 rollers inside them are used to carry the load of the bearing. The inner rollers come into contact with two different electrodes during rotation, causing the generation of electrical signals. Fig. 11g shows the effect of rotation speed on the output performance. As the rotation speed increases from 50 r/min to 600 r/min, the open circuit voltage correspondingly increases from 8 V to 60 V, showing a highly linear relationship between rotation speed and open circuit voltage. This work makes full use of the waste energy generated by the bearing operation, and realizes the accurate monitoring of the bearing working state while reducing the energy consumption. Zhang et al. [231] proposed a multi-electrode mechanical motion sensor using gear-like meshing, realizing the velocity measurement of linear motion and rotational motion. The error rate is less than 3%, and the actual monitoring performance is superior in 9 motion modes. Integrating triboelectric speed sensors into bearings is the first step towards commercial applications [232–234]. Xie et al. proposed a triboelectric rotational speed sensor (TRSS), which can measure the range of 10-1000 rpm with error less than 0.3% [233]. Fig. 11h illustrates the detailed structure of TRSS, which is mainly made up of a rotor, a stator, a bearing seat, a bearing, and an adjusting ring. When mounted on a bearing, the stator and rotor of the TRSS rotate relatively in response to the rotation of the bearing, working on the freestanding-mode and generating current signal. The industrial application of TRSS to measure rotational speed of the mechanical component is shown in Fig. 11i. TRSS does not interfere with the normal operation of the bearing, and the real-time speed of the bearing can be self-powered to monitor after the bearing is installed with TRSS. Fig. 11j shows the speed sensing ability of TRSS. There is a good linear relationship between frequency and speed, and it is in good agreement with the theoretical reference line. This work demonstrates the important progress of triboelectric velocity sensors for industrial applications. Based on planar contact and spherical contact, Jing and Zhang et al. [235] designed a speed sensor integrated into industrial bearings, which can detect rotary and linear velocities with high stability and accuracy.

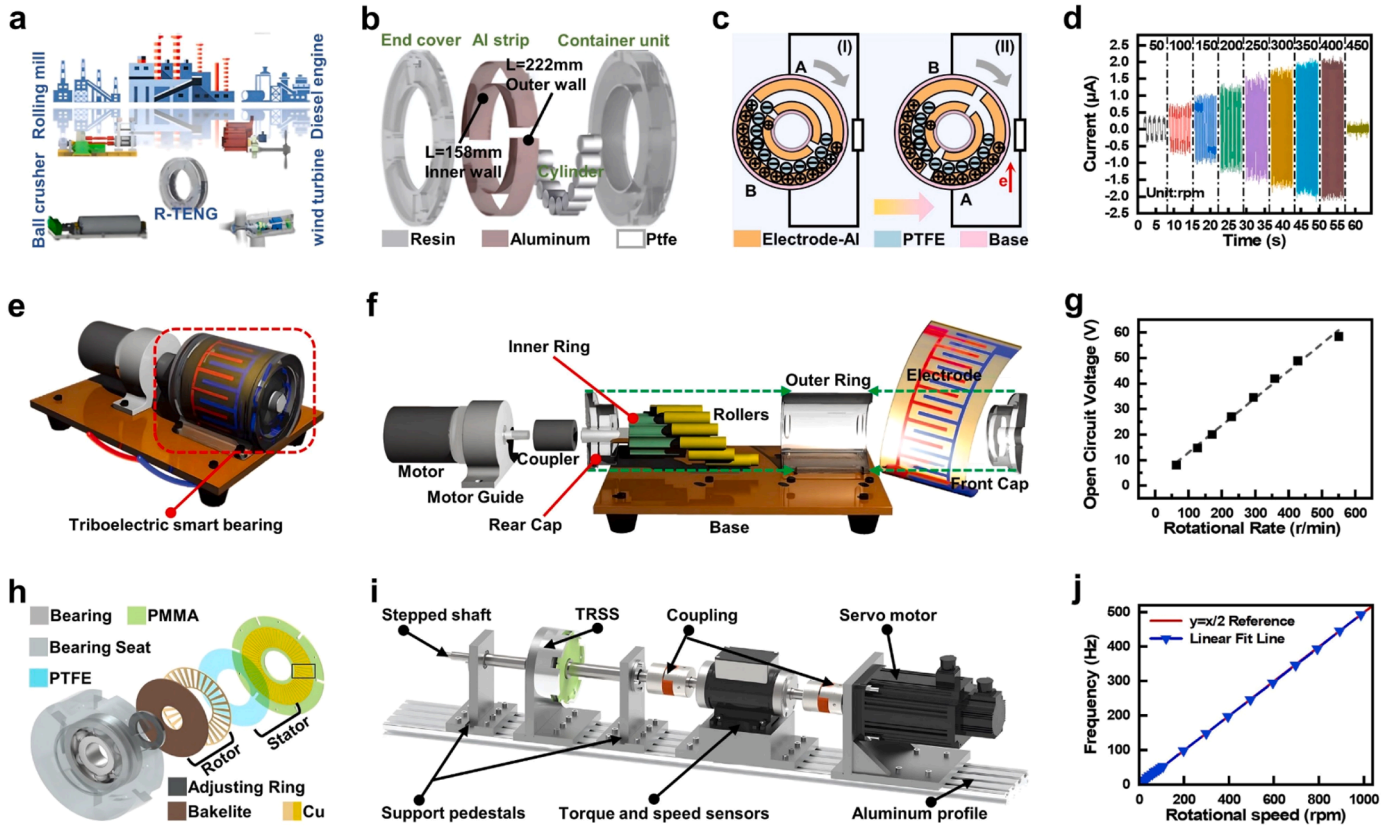

Fig. 11. The triboelectric velocity sensor: mechanical rotational speed sensor. (a) Potential application scenarios of R-TENG. (b) Structural diagram of R-TENG. (c) Working mechanism of R-TENG. (d) Output current signal of R-TENG versus different rotational speeds. Reproduced with permission from ref [229]. Copyright 2022 MDPI. (e) Schematic diagram of smart bearing. (f) Detailed structure diagram of smart bearing. (g) Relationship of rotational rate and open circuit voltage. Reproduced with permission from ref [148]. Copyright 2018 Wiley-VCH. (h) Structural diagram of TRSS. (i) TRSS utilized shafting arrangement in rotational speed measurement. (j) Linear fitting curve of frequency and rotational speed. Reproduced with permission from ref [233]. Copyright 2019 Elsevier.

In addition, Wang et al. [217] developed a non-contact sensor and the maximum error of speed measurement is only 0.2% in the range of 0-2000 RPM speed.

3.5.2. *Fluid flow velocity sensor*

The fluid flow velocity sensor is mainly used to measure the flow state of gas and liquid in the pipeline. There are two main modes of operation: film flapping and turbine-driven rotation. Among them, the membrane flapping structure is relatively simple, and the turbine rotating type is the most widely used. It can use the fluid to drive the turbine to rotate and make the TENG work passively to generate electrical signals. Firstly, Wang et al. invented a humidity-proof and wind-adapted flag-type TENG (F-TENG), which offers an alternative for sensing wind speed and direction [134]. As shown in Fig. 12a, F-TENG can convert the wind energy into electrical signals and accurately sense the wind speed in a stormy environment. Fig. 12b shows the structure and the working principle of F-TENG. F-TENG mainly consists of two carbon-coated PET films and one strip of PTFE film pasted together. When the F-TENG is excited by wind, the PTFE film alternately contacts and separates from the carbon electrode layer at both ends, thereby generating current between the two electrodes. F-TENG performs well in wind speed monitoring because the measurement results of it are not much different from those of commercial wind speed sensors, as shown in Fig. 12c. Li et al. [236] designed a wind speed sensor based on integrated wind turbine, which can detect wind speed in all directions on the plane, with a response time of 0.15 s. Moreover, Wang et al. [225] reported a new membrane flapping structure to achieve the wireless flow velocity sensing using a silver-coated polymer network liquid crystal.

For turbine-driven mode, He et al. proposed a dual-mode triboelectric nanogenerator that can be used to both collect wind energy and monitor wind speed [149]. Fig. 12d illustrates the application of dual-mode triboelectric nanogenerators, which consists of two TENGs. Two TENGs share the same stator and rotor, which can be driven by a windmill. Fig. 12e shows the 3D structural schematic of the DC-TENG. Based on the principle of electrostatic induction and electrostatic breakdown of the DC-TENG, a single-direction current is generated between the charge-collecting electrode and the triboelectric layer. Fig. 12f shows the relative linear correlation coefficient between the frequency of the output current and the wind speed, which is as high as 0.9998, indicating that the wind speed sensing performance is excellent. Rui et al. [224] proposed a self-powered active wind speed sensor that can derive wind speed from the electrical output frequency of the sensor and can detect wind speed as low as 1 $m{\cdot}s^{-1}$. In addition, Wang et al. introduced a highly adaptive hybrid nanogenerator (TEHN) [150]. The 3D explosion diagram of the TEHN is shown in Fig. 12g. TEHN mainly consists of turbine, shaft, and hybrid nanogenerator. The turbine rotates under the excitation of the fluid, and then the hybrid nanogenerator rotates with the movement of the turbine through the same shaft to convert the marine flow movement into electrical signal. Fig. 12h exhibits the potential application of TEHN. Fig. 12i shows that the correlation coefficient between the frequency of the output signal and the flow velocity is 0.98, showing a good linear relationship and indicating that the hybrid nanogenerator can be used as a flow velocity sensor. Zhang and Xi et al. [133,223] also proposed multifunctional velocity sensors that can measure wind and water flow.

To enhance the output, Cheng et al. developed a fully enclosed self-powered active spherical triboelectric sensor (SASTS) to detect the fluid velocity [116]. Fig. 12j exhibits the schematic illustration of the SASTS.

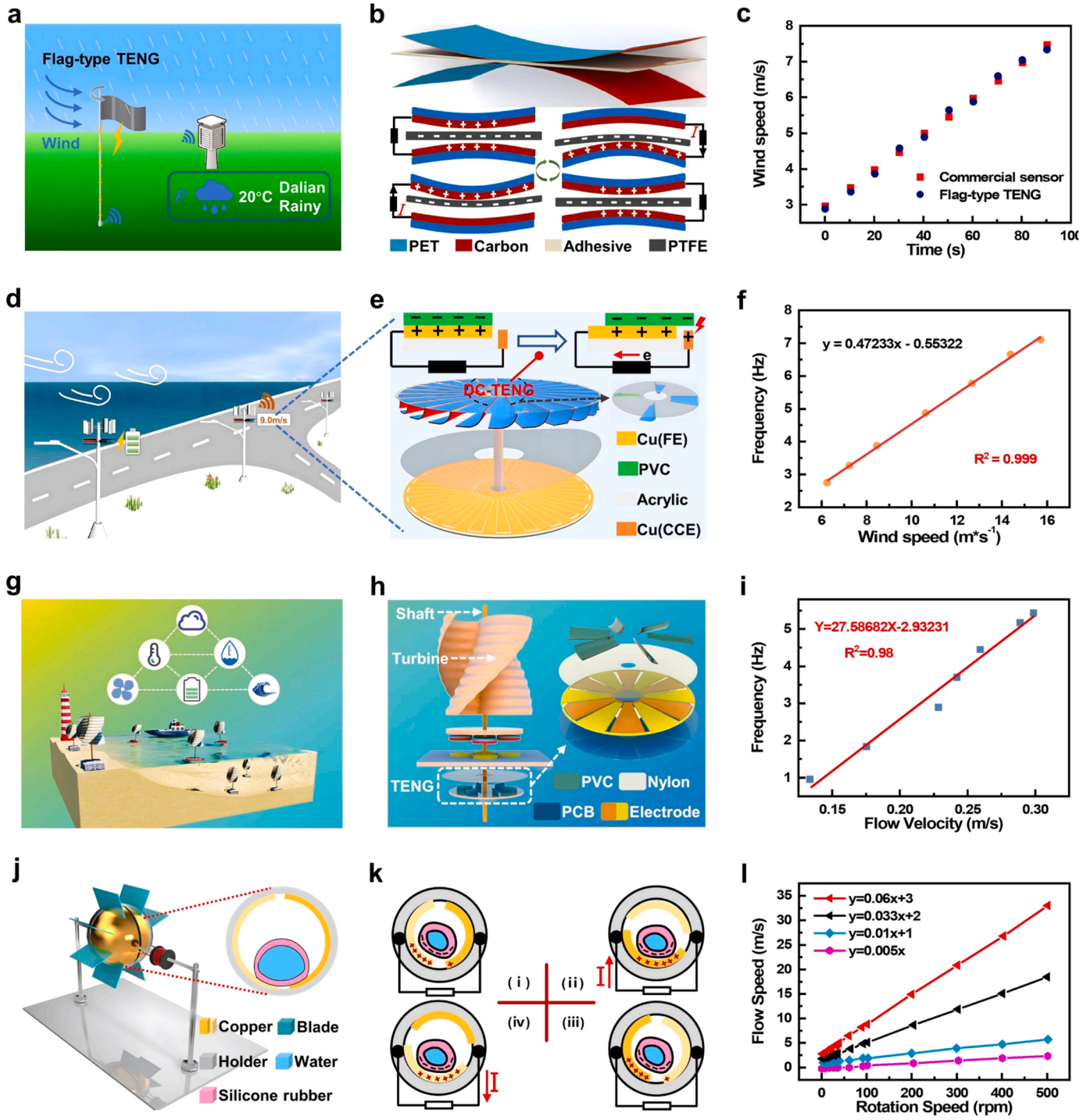

Fig. 12. The triboelectric velocity sensor: fluid flow velocity sensor. (a) Application scenarios for the flag-type TENG. (b) Structure and operating principle of the flag type TENG. (c) Comparison of flag-type TENG and commercial wind speed sensors. Reproduced with permission from ref [134]. Copyright 2020 Elsevier. (d) Scenarios in which the Dual-Mode TENG monitors wind speed in real time. (e) 3D structure of the Dual-Mode TENG and the working mechanism of the DC-TENG. (f) Linearity relationship DC-TENG at different wind speeds. Reproduced with permission from ref [149]. Copyright 2022 American Chemical Society. (g) Three-dimensional structure of TEHN. (h) Perceptual map of TEHN in the marine environment. (i) Variation of frequency with water velocity. Reproduced with permission from ref [150]. Copyright 2023 Wiley-VCH. (j) Schematic structure of the SASTS. (k) Working principle of TENH (i) Curve of flow rate with speed for different parameters. Reproduced with permission from ref [116]. Copyright 2020 IEEE.

It is made up of a spherical part, an electric brush and an outer frame, and obtains output signal by driving the blades of frame. The working principle of the SASTS is shown in Fig. 12k. Under the excitation of fluid, the internal soft ball and the electrode produce relative motion due to the rotation of the shell. The potential difference is formed between the electrodes and a current is generated in external circuit. As shown in Fig. 12l, the linear relationship of the flow velocity and the rotation speed can be adjusted by changing the parameter (like mass of sphere) of the SASTS to match various ambient environments. Therefore, SASTA can be applied to measure fluid flow velocity, and potentially even other rotational movements, such as environment monitoring. Other than that, Zhang et al. [237,238] used bionics and nano-soft materials to

develop a velocity sensor suitable for underwater low velocity according to the vortex effect of the fluid.

In conclusion, the triboelectric velocity sensor, as a sensor that can sense the rotational speed of mechanical equipment and the flow rate of fluid, can timely feedback the operating state of the equipment, enrich the information of the flow field, and improve the transparency of the marine environment. The triboelectric rotational speed sensor generally adopts the working mode of spherical contact or plane contact, which can be applied to industrial intelligent bearings to realize real-time and accurate monitoring. In addition, it can also be applied to smart ships, achieve the health monitoring of mechanical equipment, and improve the safety and reliability of equipment. Artificial intelligence and triboelectric rotational speed sensors are two innovative and forward-looking technologies in the field of industry 4.0 and intelligent manufacturing, and their combination will provide strong support for the further development of smart bearings. As a bearing unit with self-sensing, self-decision-making and self-regulation functions, intelligent bearings will be the future development direction of high-end bearings. The triboelectric flow velocity sensor generally adopts the structure of film flapping or turbine rotating, which has good sensing ability at low flow velocity and is suitable for monitoring wind speed and fluid flow velocity. The combination of artificial intelligence and triboelectric flow velocity sensors can also enable real-time monitoring and prediction of flow rates, hydrological monitoring and control of the marine environment, improve the performance and reliability of smart ships, and open up new marine resources and services. The triboelectric flow velocity sensor can also develop new sensors such as underwater low-velocity sensors through excellent bionic design and the application of soft nanomaterials, improve the perception of the underwater environment, and create an intelligent MIoT system.

4. Summary and perspectives

4.1. Summary

With the upgrading of intelligent devices and sensor networks, intelligent sensors have become the key to the competition in the high-tech field of ships. Over the past decade, TENGs have received extensive and in-depth research attention, and have been rapidly developed and applied in the field of ship and ocean engineering. This article reviews the research progress of triboelectric marine sensors in recent years, including displacement sensor, flow sensor, velocity sensor, vibration sensor and tactile sensor. Each type of marine triboelectric sensor is compared and discussed in terms of advanced structural design, material innovation, application effects and future development thinking. The representative structural design and sensing characteristics are summarized in Table 1. In view of the latest progress made by TENGs, we outline the design of a marine intelligent sensor network system to build the next generation of MIoT paradigm, as shown in Fig. 13. This intelligent sensing system includes high-performance marine triboelectric sensors, which can detect various parameters in the field of ship and ocean engineering, such as environmental information, ship attitude information, operation status information of system and equipment, etc. These sensing signals can be directly transmitted to the shore-based control center through the 5 G network. With the help of Artificial Intelligence technologies such as Digital Twins, Machine Learning, and Neural Networks, the shore-based experts can conduct sufficient analysis and modeling of the data, and provide more accurate and timely decision support for the operation and maintenance of the targeted nodes, and even remotely control through the terminals of the corresponding nodes, thereby achieving a closed-loop Internet of marine Things. It is expected that MIoT will completely change the existing working mode of the shipping industry, comprehensively improve the working efficiency of the shipping industry, and open a new era of shipping reform for us.

4.2. Perspectives

Despite recent advances in triboelectric marine sensor, there are still many challenges and opportunities that need to be addressed to achieve the intelligent sensing system. The future development of marine triboelectric sensors is a key area to be considered by academia and industry. In academia, this involves device structure, material innovation, sensitivity, reliability, waterproof, Digital Twins and Artificial Intelligence. In the industry, this involves product standardization, manufacturing, and the creation of industrial chains.

4.2.1. Academic considerations

4.2.1.1. Device structure. Through the advanced structural design, the effective contact area between tribo-materials is larger, so that the marine triboelectric sensor can accurately and effectively perceive the marine environment and ship condition information. The structural design of the sensor must first consider the motion characteristics of the detected object, through which the mode, frequency and amplitude of motion can be obtained, and then design the structure of the sensor that meets the above requirements. Then, the installation method of the sensor should be considered, and different installation methods will involve the movement mode of the internal microstructure of the sensor and the determination of the movement space range [239]. In addition, the use of 3D printing technology can turn the 3D configuration diagram designed in the computer into a physical object, and the printed configuration is relatively accurate, suitable for the assembly between miniature accessories [240].

4.2.1.2. Material innovation. The electromechanical conversion efficiency of marine triboelectric sensors depends largely on the difference of triboelectric series of triboelectric materials. Nowadays, polymer materials or compounds are commonly used as dielectric materials. However, the inherent electronic affinity of existing tribo-materials hinders further improvement of electromechanical conversion efficiency. Therefore, the use of new raw materials and the development of new composite materials are crucial to solve the problems of high electronegativity and strong charge capture and retention capabilities [241–243]. The use of environmentally unfriendly and non-recyclable new materials should be avoided, and emphasis should be placed on the development of new triboelectric materials that are resistant to high temperature and corrosion [244–246].

4.2.1.3. Sensitivity. Marine triboelectric sensor can accurately capture marine information and be used to monitor and identify the real-time status of marine equipment and marine environment. Increasing the sensitivity requires increasing the surface charge density of the triboelectric material or expanding the detection range. In order to increase the charge density, physical, chemical and biological modifications can be introduced into the material to improve the effect of electromechanical conversion. For physical modifications, surface micro-nanostructures, such as nanocolumns, nanowires, pyramid arrays, folds, laser etching, etc., can enhance surface charge and promote close contact of dielectric materials [247]. For chemical modification, the surface charge of the triboelectric material can be adjusted and enhanced by injecting, doping or coating with foreign chemical substances [248,249]. For biological modifications, novel biological materials, such as spider silk proteins, can be mined to create a new type of triboelectric layer to enhance the sensing signal [250].

4.2.1.4. Reliability. With the increasing application of marine triboelectric sensors in the maritime field, its reliability has also attracted the attention of researchers. The reliability of the sensor refers to the probability that the components and devices have specified functions within the specified time and under the specified conditions. Reliability

Table 1
A summary of structure characteristics and sensing property of the representative triboelectric marine sensors.

Sensor type	Tribo-materials	Sensing index	Measuring range	Sensitivity	Accuracy	Durability	Individual Advantages	Classification Disadvantages	Refs.
Triboelectric tactile sensor	Silicone rubber /Latex	Force	1-50 N	0.038 V/N	99.60%	5000 cycles	humidity resistance, high strain, flexibility	susceptible to environmental factors, signal drift	[101]
	conductive ink/ FEP	Amplitude	25-125 mm	/	99.06%	/	bionic coral, three-dimensional perception, millimeter accuracy		[102]
	conductive sponge/FEP	Force	50, 65, 70, 75 kg	/	94.44%	/	stable, privacy, high precision		[138]
	conductive ink /FEP	Force	0.1-0.45 N	/	99.41%	/	bionic seal tentacles, perception of hydrodynamic trajectory, high integration		[139]
	conductive ink/ FEP	Amplitude	1-5 mm	/	99.56%	300 cycles	bionic beard, underwater robot obstacle avoidance, high sensitivity		[181]
	conductive ink /FEP	Force	1-5 N	/	99%	/	bionic sea otter palm, underwater high-frequency work, multidimensional perception		[117]
Triboelectric displacement sensor	PTFE/Water	Amplitude	10-80 mm	23.5 mV/mm	/	3 Days	humidity resistance, millimeter accuracy, high sensitivity	susceptible to environmental factors, signal drift	[187]
	PTFE/Water	Amplitude	1-7 cm	10 mm	/	2000 cycles	robust, humidity resistance, millimeter accuracy		[100]
	PTFE/Cu	Amplitude	2-12 cm	2530 mV/mm	99.90%	/	multi-parameter perception, strong environmental adaptability		[140]
	PTFE/Water	Angle	2.9°-25.8°	1.72°	/	5 Days	maintenance-free, durable, high sensitivity		[99]
	Magnetic disk/PTFE	Angle	0°-360°	/	/	/	multi-parameter perception		[106]
	FEP/Cu	Angle	0° - 360°	/	/	/	cost-effective, simple manufacturing, multi-parameter perception		[141]
Triboelectric flow sensor	PTFE/Cu	Flow	5-30 m^3/h	/	2.80%	/	low pressure loss, high sensitivity, high precision	susceptible to environmental factors, prone to corrosion, signal drift	[142]
	PTFE/Cu	Flow	11-28 L/min	/	/	/	self-powered		[143]
	PTFE/Cu	Flow	30-300 L/min	>5 L/min	99.70%	/	strong environmental adaptability, high resolution, accurate and flexible		[109]
	PTFE/Particle	Flow	3-68 g/s	/	>98%	17 cycles	simple manufacturing, low cost, multi-parameter perception		[144]
	FEP/Cu and PTFE/Water	Flow	94-264 L/min	/	>98.05%	4 h	multi-parameter perception, strong environmental adaptability		[108]
	PTFE/Water	Flow	95 -215 L/min	/	99.90%	/	stable, reliable		[124]
Triboelectric vibration sensor	Kapton/Al	Acceleration	1-9.8 m/s^2	/	>94%	/	strong environmental adaptability, integrated array	susceptible to environmental factors, signal drift	[212]
	FE/TEL	Amplitude	0-30 mm	/	99%	10000 cycles	real-time detection, intelligent early warning		[145]
	Silicone rubber /carbon	Acceleration	0-23 m/s^2	/	/	30000 cycles	multi-direction perception, multi-parameter perception		[146]
	Silicone rubber /Aluminum	Acceleration	0.5-319.8 m/s^2	/	/	14 days	broadband vibration perception, multi-parameter perception		[147]
	PTFE/Cu	Amplitude	1-4.5 mm	/	/	7 days	large-scale manufacturing, stable		[11]
	Cu/Hg/PVDF	Acceleration	0-60 m/s^2	0.26 V·s/m^2	/	200000 cycles	high sensitivity, durable, robust		[14]
	FEP/Al	Acceleration	1-2000 Hz	/	99.78%	1000000 cycles	broadband vibration monitoring, high sensitivity		[103]
Triboelectric velocity sensor	PTFE/Al	Rotate speed	0-400 rpm	/	/	15000 cycles	self-powered, strong environmental adaptability	susceptible to environmental factors, signal drift	[229]
	PTFE/Al	Rotate speed	0-550 r/min	15°	/	28000 rounds	simple manufacturing, cost-effective, multi-parameter perception		[148]
	PTFE/Cu	Rotate speed	10-1000 rpm	/	>99.7%	/	high precision, high reliability, high integration		[233]

(*continued on next page*)

Table 1 (*continued*)

Sensor type	Tribo-materials	Sensing index	Measuring range	Sensitivity	Accuracy	Durability	Individual Advantages	Classification Disadvantages	Refs.
	Carbon/PTFE	Speed	2.0-7.5 m/s	/	/	/	humidity resistance, adaptive wind direction, multi-parameter perception		[134]
	PVC/Cu	Speed	3.77-11.91 m/s	/	99.90%	1500000 cycles	real-time monitoring, self-powered, durable		[149]
	PVC/Nylon	Speed	0.13-0.3 m/s	/	98%	/	self-powered, integrated array, strong adaptability		[150]
	silicone rubber /Cu	Speed	2-16 m/s	/	/	6 months	high precision, wide working range, durable		[116]

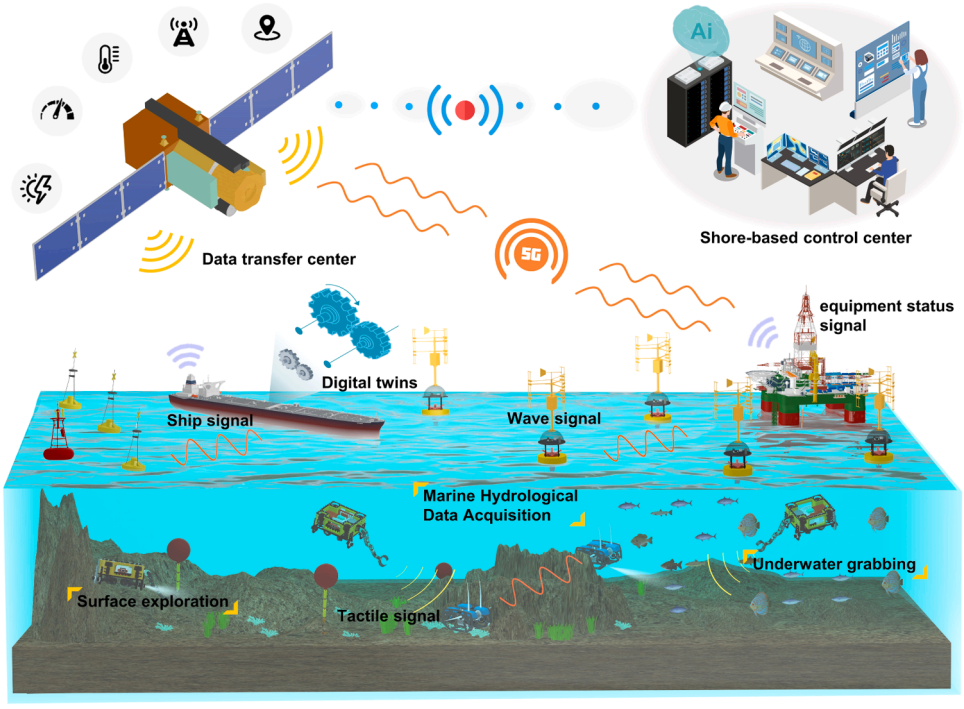

Fig. 13. Vision for the next generation of Marine Internet of Things paradigm.

is crucial for sensor applications. In the monitoring of marine environment and ship equipment condition, low reliability may lead to the failure to accurately obtain ship navigation information and the failure of ship equipment to work normally. Reliability can be determined by zero error, range, resolution, accuracy, sensitivity, precision, linearity, response time, lag, and transmission loss. For resolution, the resolution can be improved by selecting or developing tribo-materials with higher electrical sensitivity [251]. In terms of zero error, it can be avoided by measuring the response of the output signal, and during the calculation of the response, the read value after detection is subtracted from the read value before detection, thus cancelling out the zero error [252]. The improvement of accuracy, resolution and stability will all play a positive role.

4.2.1.5. Waterproof. Current marine triboelectric sensors also face serious waterproof challenges, as salt, humidity and pressure in seawater can affect the structure and performance of the TENG. Therefore, the design and implementation of effective waterproofing strategy is the key to ensure the normal operation of marine sensors. We summarize the following strategies: (1) Encapsulation. It is to wrap the marine sensor in a waterproof material to prevent seawater infiltration and corrosion. (2) Coating method. It is done by coating the surface of the TENG with a waterproof film to increase its water resistance and corrosion resistance. (3) Self-healing method. It uses some polymers or hydrogels with self-healing ability as waterproof materials for TENG, so that the TENG can automatically restore its function after major deformation or damage, reducing maintenance costs and risks. (4) Bionic method. It is to use bionic thinking, for example, by imitating the super hydrophobic waterproof properties of the lotus leaf surface, and by optimizing the material or surface treatment to make the surface of the triboelectric material have good hydrophobic properties, so that the TENG can achieve a natural waterproof effect.

4.2.1.6. Digital Twins. The application of digital twin technology in marine triboelectric sensors provides powerful data support for the perception, transmission and computing applications of marine information. By reading and fusing the real-time data of the sensor, the 3D image of the ocean is constructed, and a visual remote monitoring platform is established, which can analyze the status of the monitoring target and give timely warning and corresponding coping strategies. Through the integration of big data, cloud computing and other technologies, the data of the sensor is processed and optimized to improve the accuracy and stability of the sensor, achieve a wider range of high-precision information perception, adapt to more complex environmental changes, and provide powerful data support for various applications of marine triboelectric sensors.

4.2.1.7. Artificial Intelligence. Artificial intelligence technology can use

machine learning, deep learning, neural network to analyze and model data, so as to realize the perception and control of machinery and environmental conditions. Artificial intelligence technology can be combined with marine triboelectric sensors, which provides a powerful tool for information extraction and analysis of large-scale data. Artificial intelligence technology is used to mine and analyze the data of marine triboelectric sensors to find the rules and anomalies in marine information,providing decision support for marine scientific research and engineering applications. In addition, artificial intelligence technology can fuse and predict the data obtained by marine triboelectric sensors in real time, and realize the inversion of marine environmental hydrological information and the intelligent operation and maintenance of marine equipment.

4.2.2. Industrial considerations

4.2.2.1. Product standardization. Sensor standardization refers to the specification formulated in the aspects of technology, performance, quality, production and testing, which plays an important role in the design, production, testing and application of sensors. The new sensor standard is mainly used to ensure the performance and quality of new sensors, improve reliability, stability and interoperability, and strengthen the compatibility and interchangeability between sensors. The sensor standard includes many aspects, such as the structure, the working principle, the technical specification, the performance requirements, the test method and the application range of the sensor, and so on. The formulation of sensor standards should be based on the actual needs of countries, regions and industries to improve the technical level of sensors and promote the wide application of sensors in production and applications. With the increasing demand for marine triboelectric sensors, the standardization and internationalization of this new type of sensor will also become increasingly important to promote the development of new sensor technology and application innovation.

4.2.2.2. Manufacturing. To solve the problem of scaling up production, we propose to consider three economies-of-scale factors, including lower raw material costs and supply, a unified design production model and adaptation to existing production equipment and established agreements. Cheaper strong electrosensitive materials (PTFE or PVDF) will provide easier scalability. The manufacturing method should adopt micro-nano manufacturing technology, which takes micron or nanometer scale as the working scale, and uses micro-machining, microelectronics, micro-mechanical systems and other technologies to manufacture micro- and nano-level devices, structures and systems, such as electrospinning, etching and so on [253,254]. In addition, the existing production equipment should also be upgraded on the basis of the existing technical level to accurately manufacture the triboelectric sensor that meets the requirements of the ship [255,256].

4.2.2.3. Creation of industrial chains. Sensors are the main source of equipment and systems to perceive the external environment information, and are an important support for the development of intelligent manufacturing, robotics, industrial Internet, vehicle networking, unmanned driving, and smart cities. The sensor industry has the characteristics of small batch, multiple varieties, large structural differences, and close integration with application scenarios. Marine triboelectric sensor is a multi-component integrated circuit with functions of information acquisition, information processing, information exchange, information storage, etc. It is used to send measurement, status information, receive and process external commands. The technology of marine triboelectric sensor is developing towards embedded, miniaturized, modular, intelligent, integrated and networked [257,258]. At the same time, the industry should present a development pattern combining group monopoly and fine division of labor. Large companies can gradually form a monopoly position through merger and reorganization, occupy the high-end market and expand to the middle and low-end market, control technical standards and patents, and lead the direction of industrial development. Small enterprises can develop in the direction of "small, fine, specialized and strong", and improve the market competitiveness of products and services through outstanding advantages in market segments and cooperation at the industrial chain level.

Funding

The work was supported by the National Natural Science Foundation of China (Grant Nos. 52101400, 52101345, 51879022), the Scientific Research Fund of the Educational Department of Liaoning Province (LJKMZ20220359), the Dalian Outstanding Young Scientific and Technological Talents Project (2021RJ11).

CRediT authorship contribution statement

Sun Peiting: Writing – review & editing, Supervision. **Xu Minyi:** Writing – review & editing, Supervision, Project administration, Funding acquisition. **Du Taili:** Writing – review & editing, Funding acquisition. **Ji Yulong:** Writing – review & editing, Supervision. **Wang Yu:** Writing – review & editing. **Zhang Xinyu:** Writing – original draft, Data curation. **Feng Liang:** Supervision. **Sun Minzheng:** Writing – original draft, Visualization, Investigation, Data curation. **Li Shuang:** Writing – original draft, Data curation. **Zou Yongjiu:** Writing – original draft, Visualization, Resources, Investigation, Funding acquisition, Conceptualization.

Declaration of Competing Interest

The authors declare that they have no known competing financial interests or personal relationships that could have appeared to influence the work reported in this paper.

Data availability

Data will be made available on request.

Acknowledgements

None

Institutional Review Board Statement

Not applicable.

Informed Consent Statement

Not applicable.

References

[1] D. Liu, C. Li, P. Chen, X. Zhao, W. Tang, Z.L. Wang, Adv. Energy Mater. 13 (2022) 2202691.
[2] J. Luo, Y. Chen, M. Wu, Y. Yang, IEEE Commun. Surv. Tutor. 23 (2021) 137.
[3] N.J. Lindsey, T.C. Dawe, J.B. Ajo-Franklin, Science 366 (2019) 1103.
[4] T. Bhatta, P. Maharjan, K. Shrestha, S. Lee, M. Salauddin, M.T. Rahman, S.M. S. Rana, S. Sharma, C. Park, S.H. Yoon, J.Y. Park, Adv. Energy Mater. 12 (2022) 2102460.
[5] R.R. Negenborn, F. Goerlandt, T.A. Johansen, P. Slaets, O.A.V. Banda, T. Vanelslander, N.P. Ventikos, Nature 615 (2023) 30.
[6] X. Wang, Y. Hu, J. Li, J. Ma, N. Wan, J. Wen, T. Cheng, Sustain. Energy Technol. Assess. 54 (2022) 102824.
[7] B. Cao, P. Wang, P. Rui, X. Wei, Z. Wang, Y. Yang, X. Tu, C. Chen, Z. Wang, Z. Yang, T. Jiang, J. Cheng, Z.L. Wang, Adv. Energy Mater. 12 (2022) 2202627.
[8] C. Shan, W. He, H. Wu, S. Fu, K. Li, A. Liu, Y. Du, J. Wang, Q. Mu, B. Liu, Y. Xi, C. Hu, Adv. Funct. Mater. 33 (2023) 2305768.
[9] D. Yu, C. Sun, K. Wang, S. Yin, L. Sun, H. Chen, F. Kong, Appl. Nanosci. 12 (2022) 1697.

[10] H. Luo, K. Wu, R. Ruby, Y. Liang, Z. Guo, L.M. Ni, IEEE Commun. Surv. Tutor. 20 (2018) 2855.
[11] X. Xiao, X. Zhang, S. Wang, H. Ouyang, P. Chen, L. Song, H. Yuan, Y. Ji, P. Wang, Z. Li, Adv. Energy Mater. 9 (2019) 1902460.
[12] J. Zhao, D. Wang, F. Zhang, Y. Liu, B. Chen, Z.L. Wang, J. Pan, R. Larsson, Y. Shi, ACS nano 15 (2021) 11869.
[13] S. Xiao, H. Wu, N. Li, X. Tan, H. Deng, X. Zhang, J. Tang, Y. Li, Adv. Sci. (Weinh.) 10 (2023) e2207230.
[14] B. Zhang, L. Zhang, W. Deng, L. Jin, F. Chun, H. Pan, B. Gu, H. Zhang, Z. Lv, W. Yang, Z.L. Wang, ACS Nano 11 (2017) 7440.
[15] J. Zhao, D. Wang, F. Zhang, J. Pan, P. Claesson, R. Larsson, Y. Shi, Nanomicro Lett. 14 (2022) 160.
[16] Y. Duan, H. Xu, S. Liu, P. Chen, X. Wang, L. Xu, T. Jiang, Z.L. Wang, Nano Res. 16 (2023) 11646.
[17] X. Wang, C. Ye, P. Chen, H. Pang, C. Wei, Y. Duan, T. Jiang, Z.L. Wang, Adv. Funct. Mater. (2023) 2311196.
[18] J. Luo, Z.L. Wang, EcoMat 2 (2020) e12059.
[19] Y. Jiang, X. Liang, T. Jiang, Z. Lin Wang, Engineering (2023).
[20] J. Han, Y. Liu, Y. Feng, T. Jiang, Z.L. Wang, Adv. Energy Mater. 13 (2022) 2203219.
[21] C. Han, Z. Cao, Z. Yuan, Z. Zhang, X. Huo, L. a Zhang, Z. Wu, Z.L. Wang, Adv. Funct. Mater. 32 (2022) 2205011.
[22] W. Yuan, B. Zhang, C. Zhang, O. Yang, Y. Liu, L. He, L. Zhou, Z. Zhao, J. Wang, Z. L. Wang, One Earth. 5 (2022) 1055.
[23] T. Song, S. Jiang, N. Cai, G. Chen, Chem. Eng. J. 475 (2023) 146292.
[24] C. Zhang, Y. Hao, J. Yang, W. Su, H. Zhang, J. Wang, Z.L. Wang, X. Li, Adv. Energy Mater. 13 (2023) 2300387.
[25] E. Poloczanska, Science 359 (2018) 864.
[26] G. Marra, D.M. Fairweather, V. Kamalov, P. Gaynor, M. Cantono, S. Mulholland, B. Baptie, J.C. Castellanos, G. Vagenas, J.-O. Gaudron, J. Kronjäger, I.R. Hill, M. Schioppo, I.B. Edreira, K.A. Burrows, C. Clivati, D. Calonico, A. Curtis, Science 376 (2022) 874.
[27] M. Jahanbakht, W. Xiang, L. Hanzo, M. Rahimi, Azghadi, IEEE Commun. Surv. Tutor. 23 (2021) 904.
[28] F. Chai, K.S. Johnson, H. Claustre, X. Xing, Y. Wang, E. Boss, S. Riser, K. Fennel, O. Schofield, A. Sutton, Nat. Rev. Earth Environ. 1 (2020) 315.
[29] L. Lei, Y. Zhou, G. Yang, Inf. Fusion 94 (2023) 257.
[30] Y. Yang, J. Wen, F. Chen, Y. Hao, X. Gao, T. Jiang, B. Chen, Z.L. Wang, Adv. Funct. Mater. 32 (2022) 2200521.
[31] Y. Hou, X. Dong, D. Li, D. Shi, W. Tang, Z.L. Wang, Adv. Funct. Mater. (2023) 2305719.
[32] L.L. Zhou, D. Liu, J. Wang, Z.L. Wang, Friction 8 (2020) 481.
[33] P. Maharjan, S. Lee, T. Bhatta, G.B. Pradhan, K. Shrestha, S. Jeong, S.M.S. Rana, J. Y. Park, Adv. Mater. Technol. 8 (2022) 2201545.
[34] H. Zhao, M. Xu, M. Shu, J. An, W. Ding, X. Liu, S. Wang, C. Zhao, H. Yu, H. Wang, Nat. Commun. 13 (2022) 3325.
[35] X. Hang, T. Jiang, G.X. Liu, T.X. Xiao, L. Xu, W. Li, F.B. Xi, C. Zhang, Z.L. Wang, Adv. Funct. Mater. 29 (2019) 1807241.
[36] T. Jiang, H. Pang, J. An, P.J. Lu, Y.W. Feng, X. Liang, W. Zhong, Z.L. Wang, Adv. Energy Mater. 10 (2020) 2000064.
[37] H.J. Han, G.R. Lee, Y. Han, H. Jang, E.N. Cho, S. Kim, C.S. Kim, S. Yim, J. W. Jeong, J.M. Kim, S. Yu, H.L. Tuller, Y.S. Jung, Adv. Funct. Mater. 32 (2021) 2108891.
[38] J. Chen, S. Gong, T. Gong, X. Yang, H. Guo, Adv. Energy Mater. 13 (2023) 2203689.
[39] Q. Jiang, R. Li, F. Wang, X. Shi, F. Chen, Y. Huang, B. Wang, W. Zhang, X. Wu, F. Wei, R. Zhang, Adv. Mater. 34 (2022) 2107062.
[40] W. Zhong, L. Xu, H. Wang, J. An, Z.L. Wang, Adv. Funct. Mater. 29 (2019) 1905319.
[41] J.S. Lee, J. Oh, J. Jun, J. Jang, ACS Nano 9 (2015) 7783.
[42] L. Lin, Q. Jing, Y. Zhang, Y. Hu, S. Wang, Y. Bando, R.P.S. Han, Z.L. Wang, Energy Environ. Sci. 6 (2013) 1164.
[43] Z. Ren, X. Liang, D. Liu, X. Li, J. Ping, Z. Wang, Z.L. Wang, Adv. Energy Mater. 11 (2021) 2101116.
[44] F. Shen, Z. Li, H. Guo, Z. Yang, H. Wu, M. Wang, J. Luo, S. Xie, Y. Peng, H. Pu, Adv. Electron. Mater. 7 (2021) 2100277.
[45] K. Xia, J. Fu, Z. Xu, Adv. Energy Mater. 10 (2020) 2000426.
[46] H. Hong, X. Yang, H. Cui, D. Zheng, H. Wen, R. Huang, L. Liu, J. Duan, Q. Tang, Energy Environ. Sci. 15 (2022) 621.
[47] C. Li, S. Guo, Inf. Fusion 95 (2023) 199.
[48] A. Ahmed, J. Mater. Chem. A 10 (2022) 1992.
[49] J. Guo, J. He, Z. Yuan, J. Tao, X. Liu, Z. Song, W. Gao, C. Wang, C. Pan, Nano Energy 110 (2023) 108392.
[50] Y. Du, Q. Tang, S. Fu, C. Shan, Q. Zeng, H. Guo, C. Hu, Nano Res. 16 (2023).
[51] M. Krieg, K. Nelson, K. Mohseni, Nat. Mach. Intell. 1 (2019) 216.
[52] W. Yang, W. Gong, W. Gu, Z. Liu, C. Hou, Y. Li, Q. Zhang, H. Wang, Adv. Mater. 33 (2021) 2104681.
[53] H. Nesser, H.A. Mahmoud, G. Lubineau, Adv. Sci. (Weinh.) 10 (2023) e2301807.
[54] H.S. Kim, D.Y. Kim, J.E. Kim, J.H. Kim, D.S. Kong, G. Murillo, G.H. Lee, J.Y. Park, J.H. Jung, Adv. Funct. Mater. 29 (2019) 19055816.
[55] B.D. Chen, W. Tang, C. He, C.R. Deng, L.J. Yang, L.P. Zhu, J. Chen, J.J. Shao, L. Liu, Z.L. Wang, Mater. Today 21 (2018) 88.
[56] P. Wang, S. Zhang, L. Zhang, L. Wang, H. Xue, Z.L. Wang, Nano Energy 72 (2020) 104703.
[57] D. Kumar, X. Ding, W. Du, A. Cerpa, presented at Proceedings of the 8th ACM International Conference on Systems for Energy-Efficient Buildings, Cities, and Transportation (November). Building sensor fault detection and diagnostic system, ACM,, Coimbra Portugal, 2021.
[58] I. Lobachev, E. Cretu, presented at 2016 IEEE 7th Annual Information Technology, Electronics and Mobile Communication Conference (IEMCON) (October). Smart sensor network for smart buildings, IEEE,, Vancouver Canada, 2016.
[59] S. Wakabayashi, T. Arie, S. Akita, K. Nakajima, K. Takei, Adv. Mater. 34 (2022) 2201663.
[60] S.M. Xu, X. Liang, X.Y. Wu, S.L. Zhao, J. Chen, K.X. Wang, J.S. Chen, Nat. Commun. 10 (2019).
[61] A.A. Aziz, Y.A. Sekercioglu, P. Fitzpatrick, M. Ivanovich, IEEE Commun. Surv. Tutor. 15 (2013) 121.
[62] T. Du, F. Dong, Z. Xi, M. Zhu, Y. Zou, P. Sun, M. Xu, Small (Weinh. der Bergstr., Ger.) 19 (2023) e2300401.
[63] A. Kaswan, P.K. Jana, S.K. Das, IEEE Commun. Surv. Tutor. 24 (2022) 1750.
[64] G.T. Hwang, V. Annapureddy, J.H. Han, D.J. Joe, C. Baek, D.Y. Park, D.H. Kim, J. H. Park, C.K. Jeong, K.I. Park, J.J. Choi, D.K. Kim, J. Ryu, K.J. Lee, Adv. Energy Mater. 6 (2016) 1600237.
[65] W. Mrozik, M.A. Rajaeifar, O. Heidrich, P. Christensen, Energy Environ. Sci. 14 (2021) 6099.
[66] R. Sharifian, H.C. van der Wal, R.M. Wagterveld, D.A. Vermaas, Chem. Eng. J. 458 (2023) 141407.
[67] C.E. Reimers, M. Wolf, Y. Alleau, C. Li, J. Power Sources 522 (2022) 231033.
[68] I. Huang, Y. Zhang, H.M. Arafa, S. Li, A. Vazquez-Guardado, W. Ouyang, F. Liu, S. Madhvapathy, J.W. Song, A. Tzavelis, J. Trueb, Y. Choi, W.J. Jeang, V. Forsberg, E. Higbee-Dempsey, N. Ghoreishi-Haack, I. Stepien, K. Bailey, S. Han, Z.J. Zhang, C. Good, Y. Huang, A.J. Bandodkar, J.A. Rogers, Energy Environ. Sci. 15 (2022) 4095.
[69] I. Gonçalves, C. Rodrigues, J. Ventura, Adv. Energy Mater. (2023) 2302627.
[70] Z.L. Wang, Adv. Energy Mater. 10 (2020) 2000137.
[71] D.K. Sah, T. Amgoth, Inf. Fusion 63 (2020) 223.
[72] W. Xu, L.B. Huang, M.C. Wong, L. Chen, G. Bai, J. Hao, Adv. Energy Mater. 7 (2016) 1601529.
[73] R. Wang, S. Gao, Z. Yang, Y. Li, W. Chen, B. Wu, W. Wu, Adv. Mater. 30 (2018) 1706267.
[74] Z.L. Wang, Nano Energy 68 (2020) 104272.
[75] Z.L. Wang, Mater. Today 20 (2017) 74.
[76] Z.L. Wang, Theor. Model. Triboelectric Nanogenerators 128 (2016) 155.
[77] Z.L. Wang, Mater. Today 52 (2022) 348.
[78] T. Cheng, J. Shao, Z.L. Wang, Nat. Rev. Methods Prim. 3 (2023) 39.
[79] F. Jiang, L. Zhan, J.P. Lee, P.S. Lee, Adv. Mater. (2023) e2308197.
[80] D. Jiang, M. Lian, M. Xu, Q. Sun, B.B. Xu, H.K. Thabet, S.M. El-Bahy, M. M. Ibrahim, M. Huang, Z. Guo, Adv. Compos. Hybrid. Mater. 6 (2023) 57.
[81] D. Zhang, D. Wang, Z. Xu, X. Zhang, Y. Yang, J. Guo, B. Zhang, W. Zhao, Coord. Chem. Rev. 427 (2021) 213597.
[82] W. Tang, Q. Sun, Z.L. Wang, Chem. Rev. 123 (2023) 12105.
[83] G. Khandelwal, R. Dahiya, Adv. Mater. 34 (2022) 2200724.
[84] C. Shan, W. Liu, Z. Wang, X. Pu, W. He, Q. Tang, S. Fu, G. Li, L. Long, H. Guo, J. Sun, A. Liu, C. Hu, Energy Environ. Sci. 14 (2021) 5395.
[85] Y. Wang, H. Guo, J. Liao, Y. Qin, A. Ali, C. Li, Chem. Eng. J. 476 (2023) 146571.
[86] B. Chen, W. Tang, Z.L. Wang, Mater. Today 50 (2021) 224.
[87] K. Ghosh, C. Iffelsberger, M. Konečný, J. Vyskočil, J. Michalička, M. Pumera, Adv. Energy Mater. 13 (2023) 2203476.
[88] H. Xu, X. Wang, Y. Nan, H. Zhou, Y. Wu, M. Wang, W. Liu, J. Duan, Y. Huang, B. Hou, Adv. Funct. Mater. 33 (2023) 2304723.
[89] L. Liu, M. Wu, W. Zhao, J. Tao, X. Zhou, J. Xiong, Adv. Funct. Mater. (2023) 2308353.
[90] C. Xu, Y. Liu, Y. Liu, Y. Zheng, Y. Feng, B. Wang, X. Kong, X. Zhang, D. Wang, Appl. Mater. Today 20 (2020) 100645.
[91] J. Han, Y. Liu, Y. Feng, T. Jiang, Z.L. Wang, Adv. Energy Mater. 13 (2023) 2203219.
[92] C. Rodrigues, D. Nunes, D. Clemente, N. Mathias, J.M. Correia, P. Rosa-Santos, F. Taveira-Pinto, T. Morais, A. Pereira, J. Ventura, Energy Environ. Sci. 13 (2020) 2657.
[93] J. Ahn, J.S. Kim, Y. Jeong, S. Hwang, H. Yoo, Y. Jeong, J. Gu, M. Mahato, J. Ko, S. Jeon, J.H. Ha, H.S. Seo, J. Choi, M. Kang, C. Han, Y. Cho, C.H. Lee, J.H. Jeong, I.K. Oh, I. Park, Adv. Energy Mater. 12 (2022) 2201341.
[94] Y. Zhang, Y. Li, R. Cheng, S. Shen, J. Yi, X. Peng, C. Ning, K. Dong, Z.L. Wang, Research 2022 (2022) 9809406.
[95] Z. Deng, L. Xu, H. Qin, X. Li, J. Duan, B. Hou, Z.L. Wang, Adv. Mater. 34 (2022) 2205064.
[96] A. Yu, M. Song, Y. Zhang, Y. Zhang, L. Chen, J. Zhai, Z.L. Wang, Nano Res. 8 (2014) 765.
[97] A. Ahmed, Z. Saadatnia, I. Hassan, Y.L. Zi, Y. Xi, X. He, J. Zu, Z.L. Wang, Adv. Energy Mater. 7 (2017) 1601705.
[98] Y. Wang, X. Liu, T. Chen, H. Wang, C. Zhu, H. Yu, L. Song, X. Pan, J. Mi, C. Lee, M. Xu, Nano Energy 90 (2021) 106503.
[99] S. Wang, Y. Wang, D. Liu, Z. Zhang, W. Li, C. Liu, T. Du, X. Xiao, L. Song, H. Pang, M. Xu, Sens. Actuators A: Phys. 317 (2021) 112459.
[100] X. Zhang, M. Yu, Z. Ma, H. Ouyang, Y. Zou, S.L. Zhang, H. Niu, X. Pan, M. Xu, Z. Li, Z.L. Wang, Adv. Funct. Mater. 29 (2019) 1900327.
[101] C. Zhao, D. Liu, Y. Wang, Z. Hu, Q. Zhang, Z. Zhang, H. Wang, T. Du, Y. Zou, H. Yuan, X. Pan, J. Mi, M. Xu, Nano Energy 94 (2022) 106926.
[102] X. Wang, J. Liu, S. Wang, J. Zheng, T. Guan, X. Liu, T. Wang, T. Chen, H. Wang, G. Xie, P. Xu, J. Tao, M. Xu, Adv. Mater. Technol. 7 (2021) 2101098.

[103] H. Zhao, M. Shu, Z. Ai, Z. Lou, K.W. Sou, C. Lu, Y. Jin, Z. Wang, J. Wang, C. Wu, Y. Cao, X. Xu, W. Ding, Adv. Energy Mater. 12 (2022) 2201132.
[104] H. Wu, Z. Wang, B. Zhu, H. Wang, C. Lu, M. Kang, S. Kang, W. Ding, L. Yang, R. Liao, Adv. Energy Mater. 13 (2023) 2300051.
[105] P. Wang, R. Liu, W. Ding, P. Zhang, L. Pan, G. Dai, H. Zou, K. Dong, C. Xu, Z. L. Wang, Adv. Funct. Mater. 28 (2018) 1705808.
[106] Z. Wu, W. Ding, Y. Dai, K. Dong, C. Wu, L. Zhang, Z. Lin, J. Cheng, Z.L. Wang, ACS nano 12 (2018) 5726.
[107] C. Wu, A.C. Wang, W. Ding, H. Guo, Z.L. Wang, Adv. Energy Mater. 9 (2019) 1802906.
[108] S. He, Z. Wang, X. Zhang, Z. Yuan, Y. Sun, T. Cheng, Z.L. Wang, ACS Appl. Mater. Interfaces 14 (2022) 2825.
[109] Z. Wang, Q. Gao, Y. Wang, J. Wang, Y. Wang, T. Cheng, Z.L. Wang, Adv. Mater. Technol. 4 (2019) 1900704.
[110] Y. Xu, W. Yang, X. Lu, Y. Yang, J. Li, J. Wen, T. Cheng, Z.L. Wang, ACS nano 15 (2021) 16368.
[111] Z. Wang, Y. Yu, Y. Wang, X. Lu, T. Cheng, G. Bao, Z.L. Wang, ACS Nano 14 (2020) 5981.
[112] X.P. Fu, T.Z. Bu, F.B. Xi, T.H. Cheng, C. Zhang, Z.L. Wang, ACS Appl. Mater. Interfaces 9 (2017) 32352.
[113] B. Zhang, Z. Wu, Z. Lin, H. Guo, F. Chun, W. Yang, Z.L. Wang, Mater. Today 43 (2021) 37.
[114] W.Q. Yang, J. Chen, Q.S. Jing, J. Yang, X.N. Wen, Y.J. Su, G. Zhu, P. Bai, Z. L. Wang, Adv. Funct. Mater. 24 (2014) 4090.
[115] C. Ge, J. Ma, Y. Hu, J. Li, Y. Zhang, X. He, T. Cheng, J. Wen, Adv. Mater. Technol. 8 (2022) 2201296.
[116] P. Cheng, M. Sun, C. Zhang, H. Guo, J. Shi, Y. Zhang, Y. Liu, J. Wang, Z. Wen, X. Sun, IEEE Trans. Nanotechnol. 19 (2020) 230.
[117] P. Xu, J. Liu, X. Liu, X. Wang, J. Zheng, S. Wang, T. Chen, H. Wang, C. Wang, X. Fu, G. Xie, J. Tao, M. Xu, npj Flex. Electron. 6 (2022) 25.
[118] K. Dai, X. Miao, W. Zhang, X. Huang, H. Zhang, S.W. Kim, Adv. Sci. 10 (2023) 2204694.
[119] Y. Yang, H. Zhang, J. Chen, Q. Jing, Y.S. Zhou, X. Wen, Z.L. Wang, Acs Nano 7 (2013) 7342.
[120] Z. Zhou, Z. Xu, L.N.Y. Cao, H. Sheng, C. Li, Y. Shang, W. Tang, Z.L. Wang, Adv. Funct. Mater. (2023) 2311839.
[121] K. Dai, X. Miao, W. Zhang, X. Huang, H. Zhang, S.W. Kim, Adv. Sci. 10 (2022) 2204694.
[122] X. Yin, D. Liu, L. Zhou, X. Li, G. Xu, L. Liu, S. Li, C. Zhang, J. Wang, Z.L. Wang, Adv. Funct. Mater. (2020) 2002547.
[123] J. Chen, H. Guo, J. Zheng, Y. Huang, G. Liu, C. Hu, Z.L. Wang, ACS nano 10 (2016) 8104.
[124] Y. Wang, Z. Wang, D. Zhao, X. Yu, T. Cheng, G. Bao, Z. Wang, Mater. Today Phys. 18 (2021) 100372.
[125] Y. Zhong, H. Zhao, Y. Guo, P. Rui, S. Shi, W. Zhang, Y. Liao, P. Wang, Z.L. Wang, Adv. Mater. Technol. 4 (2019) 1900741.
[126] L. Yang, J. Yu, Y. Guo, S. Chen, K. Tan, S. Li, Adv. Funct. Mater. 33 (2023) 2302147.
[127] Y. Su, G. Zhu, W. Yang, J. Yang, J. Chen, Q. Jing, Z. Wu, Y. Jiang, Z.L. Wang, ACS Nano 8 (2014) 3843.
[128] I. Mehamud, P. Marklund, M. Björling, Y. Shi, Nano Energy 98 (2022) 107292.
[129] P. Wu, F. Wang, S. Xu, T. Liu, Y. Qi, X. Zhao, C. Zhang, X. Mu, Adv. Sci. (Weinh.) 10 (2023) e2301199.
[130] J. Zou, M. Zhang, J. Huang, J. Bian, Y. Jie, M. Willander, X. Cao, N. Wang, Z. L. Wang, Adv. Energy Mater. 8 (2018) 1702671.
[131] S. Li, S. Deng, R. Xu, D. Liu, Y. Nan, Z. Zhang, Y. Gao, H. Lv, M. Li, Q. Zhang, J. Wang, Z.L. Wang, ACS Energy Lett. 7 (2022) 3080.
[132] H.L. Gao, Z.Y. Wang, C. Cui, J.Z. Bao, Y.B. Zhu, J. Xia, S.M. Wen, H.A. Wu, S. H. Yu, Adv. Mater. 33 (2021) 2102724.
[133] Y. Xi, H. Guo, Y. Zi, X. Li, J. Wang, J. Deng, S. Li, C. Hu, X. Cao, Z.L. Wang, Adv. Energy Mater. 7 (2017) 1602397.
[134] Y. Wang, E. Yang, T. Chen, J. Wang, Z. Hu, J. Mi, X. Pan, M. Xu, Nano Energy 78 (2020) 105279.
[135] X. Yu, S. Fu, X. Zuo, J. Zeng, C. Shan, W. He, W. Li, C. Hu, Adv. Funct. Mater. 32 (2022) 2207498.
[136] X. Fu, S. Xu, Y. Gao, X. Zhang, G. Liu, H. Zhou, Y. Lv, C. Zhang, Z.L. Wang, ACS Energy Lett. 6 (2021) 2343.
[137] Y. Hu, C. Xu, Y. Zhang, L. Lin, R.L. Snyder, Z.L. Wang, Adv. Mater. 23 (2011) 4068.
[138] Y. Wang, Z. Hu, J. Wang, X. Liu, Q. Shi, Y. Wang, L. Qiao, Y. Li, H. Yang, J. Liu, L. Zhou, Z. Yang, C. Lee, M. Xu, ACS Appl. Mater. Interfaces 14 (2022) 24832.
[139] S. Wang, P. Xu, X. Wang, J. Zheng, X. Liu, J. Liu, T. Chen, H. Wang, G. Xie, J. Tao, M. Xu, Nano Energy 97 (2022) 107210.
[140] C. Zhang, L. Liu, L. Zhou, X. Yin, X. Wei, Y. Hu, Y. Liu, S. Chen, J. Wang, Z. L. Wang, A.C.S. Nano 14 (2020) 7092.
[141] Y. Wu, Q. Jing, J. Chen, P. Bai, J. Bai, G. Zhu, Y. Su, Z.L. Wang, Adv. Funct. Mater. 25 (2015) 2166.
[142] T.K. Phan, S. Wang, Y. Wang, H. Wang, X. Xiao, X. Pan, M. Xu, J. Mi, Sensors 20 (2020) 729.
[143] J. Chen, W. Tang, K. Han, L. Xu, B. Chen, T. Jiang, Z.L. Wang, Adv. Mater. Technol. 4 (2019) 1800560.
[144] Y. Wang, D. Liu, Z. Hu, T. Chen, Z. Zhang, H. Wang, T. Du, S.L. Zhang, Z. Zhao, T. Zhou, M. Xu, Adv. Mater. Technol. 6 (2021) 2001270.
[145] S. Li, D. Liu, Z. Zhao, L. Zhou, X. Yin, X. Li, Y. Gao, C. Zhang, Q. Zhang, J. Wang, Z.L. Wang, ACS Nano. 14 (2020) 2475.
[146] M. Xu, P. Wang, Y.C. Wang, S.L. Zhang, A.C. Wang, C. Zhang, Z. Wang, X. Pan, Z. L. Wang, Adv. Energy Mater. 8 (2017) 1702432.
[147] T. Du, B. Ge, A.E. Mtui, C. Zhao, F. Dong, Y. Zou, H. Wang, P. Sun, M. Xu, Nanomaterials 12 (2022) 1248.
[148] D. Choi, T. Sung, J.Y. Kwon, Adv. Mater. Technol. 3 (2018).
[149] C.Z. Lixia He, Baofeng Zhang, Ou Yang, Wei Yuan, Linglin Zhou, Zhihao Zhao, Zhiyi Wu, a Z.L.W. Jie Wang, ACS Nano 16 (2022) 6244.
[150] Y. Wang, Z. Qian, C. Zhao, Y. Wang, K. Jiang, J. Wang, Z. Meng, F. Li, C. Zhu, P. Chen, H. Wang, M. Xu, Adv. Mater. Technol. 8 (2022) 2201245.
[151] Z.L. Wang, L. Lin, J. Chen, S. Niu, Y. Zi, Triboelectric Nanogenerators, Springer,, Berlin, Germany, 2016.
[152] Z.L. Wang, Mater. Today 52 (2022) 348.
[153] S. Li, J. Nie, Y. Shi, X. Tao, F. Wang, J. Tian, S. Lin, X. Chen, Z.L. Wang, Adv. Mater. 32 (2020) 2001307.
[154] Y. Zhou, W. Deng, J. Xu, J. Chen, Cell Rep. Phys. Sci. 1 (2020) 100142.
[155] C. Xu, Y. Zi, A.C. Wang, H. Zou, Y. Dai, X. He, P. Wang, Y.C. Wang, P. Feng, D. Li, Adv. Mater. 30 (2018) 1706790.
[156] H. Wu, W. He, C. Shan, Z. Wang, S. Fu, Q. Tang, H. Guo, Y. Du, W. Liu, C. Hu, Adv. Mater. 34 (2022) e2109918.
[157] P. Jiang, L. Zhang, H. Guo, C. Chen, C. Wu, S. Zhang, Z.L. Wang, Adv. Mater. 31 (2019) 1902793.
[158] L. Zhou, D. Liu, Z. Zhao, S. Li, Y. Liu, L. Liu, Y. Gao, Z.L. Wang, J. Wang, Adv. Energy Mater. 10 (2020) 2002920.
[159] C. Shan, W. He, H. Wu, S. Fu, Q. Tang, Z. Wang, Y. Du, J. Wang, H. Guo, C. Hu, Adv. Energy Mater. 12 (2022) 2200963.
[160] S. Du, S. Fu, W. He, Q. Li, K. Li, H. Wu, J. Wang, C. Shan, Q. Mu, C. Hu, Adv. Funct. Mater. 33 (2023) 2306491.
[161] L.A. Zhang, S. Liu, J. Wen, X. Huo, B. Cheng, Z. Wu, L. Wang, Y. Qin, Z.L. Wang, Energy Environ. Sci. 16 (2023) 3781.
[162] S. Xu, G. Liu, J. Wang, H. Wen, S. Cao, H. Yao, L. Wan, Z.L. Wang, Adv. Energy Mater. 12 (2022) 2103408.
[163] S. Fu, W. He, Q. Tang, Z. Wang, W. Liu, Q. Li, C. Shan, L. Long, C. Hu, H. Liu, Adv. Mater. 34 (2021) 2105882.
[164] S. Niu, S. Wang, L. Lin, Y. Liu, Y.S. Zhou, Y. Hu, Z.L. Wang, Energy Environ. Sci. 6 (2013) 3576.
[165] S. Niu, Z.L. Wang, Nano Energy 14 (2015) 161.
[166] W. Song, B. Gan, T. Jiang, Y. Zhang, A. Yu, H. Yuan, N. Chen, C. Sun, Z.L. Wang, A.C.S. Nano 10 (2016) 8097.
[167] Q. Zheng, B. Shi, F. Fan, X. Wang, L. Yan, W. Yuan, S. Wang, H. Liu, Z. Li, Z. L. Wang, Adv. Mater. 26 (2014) 5851.
[168] W. Seung, M.K. Gupta, K.Y. Lee, K.S. Shin, J.H. Lee, T.Y. Kim, S. Kim, J. Lin, J. H. Kim, S.W. Kim, Acs Nano 9 (2015) 3501.
[169] X. Li, L. Xu, P. Lin, X. Yang, H. Wang, H. Qin, Z.L. Wang, Energy Environ. Sci. 16 (2023) 3040.
[170] T. Jin, Z. Sun, L. Li, Q. Zhang, M. Zhu, Z. Zhang, G. Yuan, T. Chen, Y. Tian, X. Hou, C. Lee, Nat. Commun. 11 (2020) 5381.
[171] T. Chen, Q. Shi, M. Zhu, T. He, L. Sun, L. Yang, C. Lee, ACS Nano 12 (2018) 11561.
[172] J. Qu, Q. Yuan, Z. Li, Z. Wang, F. Xu, Q. Fan, M. Zhang, X. Qian, X. Wang, X. Wang, M. Xu, Nano Energy 111 (2023) 108387.
[173] P. Xu, J. Zheng, J. Liu, X. Liu, X. Wang, S. Wang, T. Guan, X. Fu, M. Xu, G. Xie, Z. L. Wang, Research 6 (2023) 0062.
[174] P. Xu, X. Wang, S. Wang, T. Chen, J. Liu, J. Zheng, W. Li, M. Xu, J. Tao, G. Xie, Research 2021 (2021).
[175] Y. Yang, Q. Shi, Z. Zhang, X. Shan, B. Salam, C. Lee, InfoMat 5 (2023) e12360.
[176] Q. Shi, Z. Zhang, Y. Yang, X. Shan, B. Salam, C. Lee, ACS nano 15 (2021) 18312.
[177] J. Yan-qing, X. Jian-xin, L. Ye, C. Jian, L. Yue-ming, H. Dongdong, presented at International Conference on Marine Equipment & Technology and Sustainable Development. AUV Applications and Technologies of Deep Sea Exploration in the Arctic: A Review, Springer,, Beijing China, , 2023.
[178] L. Wang, D. Zhu, W. Pang, Y. Zhang, Ocean Eng. 278 (2023) 114393.
[179] J. Rosen, Science 362 (2018) 507.
[180] Y. Zou, P.C. Tan, B.J. Shi, H. Ouyang, D.J. Jiang, Z. Liu, H. Li, M. Yu, C. Wang, X. C. Qu, L.M. Zhao, Y.B. Fan, Z.L. Wang, Z. Li, Nat. Commun. 10 (2019).
[181] J. Liu, P. Xu, J. Zheng, X. Liu, X. Wang, S. Wang, T. Guan, G. Xie, M. Xu, Nano Energy 101 (2022) 107633.
[182] Y. Dong, N. Wang, D. Yang, J. Wang, W. Lu, D. Wang, Adv. Funct. Mater. 33 (2023) 2300764.
[183] W. Hou, X. Tang, L. Fang, Q. Zheng, X. Chen, L. Zheng, Nano Energy 99 (2022) 107430.
[184] C. He, B.D. Chen, T. Jiang, L. Xu, C.B. Han, G.Q. Gu, Z.L. Wang, Adv. Mater. Technol. 3 (2018) 1700251.
[185] S.H. Chung, J. Chung, M. Song, S. Kim, D. Shin, Z.H. Lin, B. Koo, D. Kim, J. Hong, S. Lee, Adv. Energy Mater. 11 (2021) 2100936.
[186] J. An, Z. Wang, T. Jiang, P. Chen, X. Liang, J. Shao, J. Nie, M. Xu, Z.L. Wang, Mater. Today 41 (2020) 10.
[187] M. Xu, S. Wang, S.L. Zhang, W. Ding, P.T. Kien, C. Wang, Z. Li, X. Pan, Z.L. Wang, Nano Energy 57 (2019) 574.
[188] L. Xu, Y. Tang, C. Zhang, F. Liu, J. Chen, W. Xuan, H. Jin, Z. Ye, Z. Cao, Y. Li, X. Wang, S. Dong, J. Luo, Nano Res. 15 (2022) 5425.
[189] X. Liang, S. Liu, Z. Ren, T. Jiang, Z.L. Wang, Adv. Funct. Mater. 32 (2022) 2205313.
[190] L. Fang, Q. Zheng, W. Hou, J. Gu, L. Zheng, Sens. Actuators A: Phys. 349 (2023) 114015.
[191] T. Du, F. Dong, M. Zhu, Z. Xi, F. Li, Y. Zou, P. Sun, M. Xu, J. Mar. Sci. Eng. 10 (2022) 1416.

[192] X. Zhang, Y. Dong, X. Xu, H. Qin, D. Wang, Sci. China Technol. Sci. 65 (2021) 282.
[193] W. Wang, Y. Wu, Z. Chang, F. Chen, H. Wang, G. Gu, H. Zheng, G. Cheng, Z. L. Wang, ACS Appl. Mater. Interfaces 11 (2019) 6396.
[194] G. Cheng, Z.-H. Lin, Z.-l Du, Z.L. Wang, Acs Nano 8 (2014) 1932.
[195] X. Wang, C. Zhu, M. Wu, J. Zhang, P. Chen, H. Chen, C. Jia, X. Liang, M. Xu, Sens. Actuators A: Phys. 344 (2022) 113727.
[196] S. Xu, Y. Feng, Y. Liu, Z. Wu, Z. Zhang, M. Feng, S. Zhang, G. Sun, D. Wang, Nano Energy 85 (2021) 106023.
[197] G.Q. Gu, C.B. Han, Y. Bai, T. Jiang, C. He, B.D. Chen, Z.L. Wang, Adv. Mater. Technol. 3 (2018) 1800009.
[198] L. Wang, J. Li, J. Tao, M. Hu, Z. Dai, Nano Energy 89 (2021) 106393.
[199] X. Gao, M. Huang, G. Zou, X. Li, Y. Wang, Nano Energy 111 (2023) 108356.
[200] T. Du, F. Dong, R. Xu, Y. Zou, H. Wang, X. Jiang, Z. Xi, H. Yuan, Y. Zhang, P. Sun, M. Xu, Adv. Mater. Technol. 7 (2022) 2200003.
[201] J.Y. Wang, L. Pan, H.Y. Guo, B.B. Zhang, R.R. Zhang, Z.Y. Wu, C.S. Wu, L.J. Yang, R.J. Liao, Z.L. Wang, Adv. Energy Mater. 9 (2019) 1802892.
[202] Z. Wang, Y. Jin, C. Lu, J. Wang, Z. Song, X. Yang, Y. Cao, Y. Zi, Z.L. Wang, W. Ding, Energy Environ. Sci. 15 (2022) 2983.
[203] W. Jiang, C. Chen, C. Wang, J. Li, M. Zhao, T. Xiang, P. Wang, Energy Environ. Sci. 16 (2023) 6003.
[204] N. Cui, C. Dai, J. Liu, L. Gu, R. Ge, T. Du, Z. Wang, Y. Qin, Energy Environ. Sci. 13 (2020) 2069.
[205] K.W. Han, J.N. Kim, A. Rajabi-Abhari, V.T. Bui, J.S. Kim, D. Choi, I.K. Oh, Adv. Energy Mater. 11 (2020) 2002929.
[206] Y. Zou, M. Sun, W. Xu, X. Zhao, T. Du, P. Sun, M. Xu, J. Mar. Sci. Eng. 10 (2022) 1348.
[207] Z. Xu, D. Li, K. Wang, Y. Liu, J. Wang, Z. Qiu, C. Wu, J. Lin, T. Guo, F. Li, Appl. Energy 312 (2022) 118739.
[208] Q. Shi, Z. Zhao, J. Yang, H. Gui, M. Cai, C. Yao, Chem. Eng. J. 477 (2023) 146886.
[209] C. Liu, Y. Wang, N. Zhang, X. Yang, Z. Wang, L. Zhao, W. Yang, L. Dong, L. Che, G. Wang, Nano Energy 67 (2020) 104228.
[210] Q. Shi, H. Wu, H. Wang, H. Wu, C. Lee, Adv. Energy Mater. 7 (2017) 1701300.
[211] H. Zhang, Y. Yang, Y. Su, J. Chen, K. Adams, S. Lee, C. Hu, Z.L. Wang, Adv. Funct. Mater. 24 (2014) 1401.
[212] Y. Hu, J. Yang, Q. Jing, S. Niu, W. Wu, Z. Wang, ACS Nano 7 (2013) 10424.
[213] Y. Qi, Y. Kuang, Y. Liu, G. Liu, J. Zeng, J. Zhao, L. Wang, M. Zhu, C. Zhang, Appl. Energy 327 (2022) 120092.
[214] Z. Ren, L. Wu, J. Zhang, Y. Wang, Y. Wang, Q. Li, F. Wang, X. Liang, R. Yang, ACS Appl. Mater. Interfaces 14 (2022) 5497.
[215] Z. Zhang, J. He, T. Wen, C. Zhai, J. Han, J. Mu, W. Jia, B. Zhang, W. Zhang, X. Chou, C. Xue, Nano Energy 33 (2017) 88.
[216] Z. Lin, C. Sun, W. Liu, E. Fan, G. Zhang, X. Tan, Z. Shen, J. Qiu, J. Yang, Nano Energy 90 (2021) 106366.
[217] Z. Wang, F. Zhang, T. Yao, N. Li, X. Li, J. Shang, Sensors 20 (2020) 4947.
[218] X. Fu, Y. Qin, Z. Zhang, G. Liu, J. Cao, B. Fan, Z. Wang, Z. Wang, C. Zhang, Energy Environ. Mater. 0 (2023) e12566.
[219] P. Chen, J. An, S. Shu, R. Cheng, J. Nie, T. Jiang, Z.L. Wang, Adv. Energy Mater. 11 (2021) 2003066.
[220] H. Zhang, Q. Cheng, X. Lu, W. Wang, Z.L. Wang, C. Sun, Nano Energy 79 (2021) 105455.
[221] G. Ma, B. Li, S. Niu, J. Zhang, D. Wang, Z. Wang, L. Zhou, Q. Liu, L. Liu, J. Wang, Z. Han, L. Ren, Nano Energy 91 (2022) 106637.
[222] D. Zhu, X. Guo, H. Li, Z. Yuan, X. Zhang, T. Cheng, Nano Energy 108 (2023) 108233.
[223] Q. Zhang, L. Li, T. Wang, Y. Jiang, Y. Tian, T. Jin, T. Yue, C. Lee, Nano Energy 90 (2021) 106501.
[224] P. Rui, D. Li, Z. Zi, Y. Zhao, Adv. Mater. Technol. 8 (2022) 2200860.
[225] J. Wang, P. Liu, C. Meng, H.S. Kwok, Y. Zi, ACS Appl. Mater. Interfaces 13 (2021) 21450.
[226] J.S. Kim, J. Kim, J.N. Kim, J. Ahn, J.H. Jeong, I. Park, D. Kim, I.K. Oh, Adv. Energy Mater. 12 (2021) 2103076.
[227] C. Zhu, M. Wu, C. Liu, C. Xiang, R. Xu, H. Yang, Z. Wang, Z. Wang, P. Xu, F. Xing, H. Wang, M. Xu, Adv. Energy Mater. 13 (2023) 2301665.
[228] J. Sun, L. Zhang, X. Hui, Y. Huang, J. Chen, C. Hu, H. Guo, S. Qi, Z.L. Wang, Adv. Funct. Mater. 33 (2022) 2212248.
[229] Y. Xin, T. Du, C. Liu, Z. Hu, P. Sun, M. Xu, Micromachines 13 (2022) 556.
[230] Q.K. Han, Z. Ding, Z.Y. Qin, T.Y. Wang, X.P. Xu, F.L. Chu, Nano Energy 67 (2020) 104277.
[231] X. Zhang, H. Li, Q. Gao, Z. Yuan, S. He, X. Yu, Z.L. Wang, T. Cheng, Nano Energy 108 (2023) 108239.
[232] M. Gao, T. Sun, Y. Li, Z. Zhang, C. Lee, J. Choi, Adv. Funct. Mater. 33 (2023) 2304070.
[233] Z. Xie, J. Dong, Y. Li, L. Gu, B. Song, T. Cheng, Z.L. Wang, Extrem. Mech. Lett. 34 (2020) 100595.
[234] Y. Zhang, W. Wang, X. Wu, Y. Lei, J. Cao, C. Bowen, S. Bader, B. Yang, Renew. Sustain. Energy Rev. 183 (2023) 113446.
[235] Q.S. Jing, G. Zhu, W.Z. Wu, P. Bai, Y.N. Xie, R.P.S. Han, Z.L. Wang, Nano Energy 10 (2014) 305.
[236] W. Li, H. Guo, Y. Xi, C. Wang, M.S. Javed, X. Xia, C. Hu, RSC Adv. 7 (2017) 23208.
[237] S. Zhang, Z. Jing, X. Wang, K. Fan, H. Zhao, Z.L. Wang, T. Cheng, ACS Energy Lett. 7 (2022) 4282.
[238] S. Zhang, Z. Jing, X. Wang, M. Zhu, X. Yu, J. Zhu, T. Cheng, H. Zhao, Z.L. Wang, Nano Res. 16 (2022) 466.
[239] K. Zhang, Y. Wang, Y. Yang, Adv. Funct. Mater. 29 (2019) 1806435.
[240] H. Liu, H. Zhang, W. Han, H. Lin, R. Li, J. Zhu, W. Huang, Adv. Mater. 33 (2021) 2004782.
[241] J. Wei, P. Xiao, T. Chen, Adv. Mater. 35 (2023) 2211758.
[242] X. Gao, F. Xing, F. Guo, W. Sun, J. Wen, Z.L. Wang, B. Chen, Chem. Eng. J. 477 (2023) 147186.
[243] S. Fu, C. Hu, Adv. Funct. Mater. (2023) 2308138.
[244] L. Shi, V.S. Kale, Z. Tian, X. Xu, Y. Lei, S. Kandambeth, Y. Wang, P.T. Parvatkar, O. Shekhah, M. Eddaoudi, H.N. Alshareef, Adv. Funct. Mater. 33 (2023) 2212891.
[245] J. Wen, B. Chen, W. Tang, T. Jiang, L. Zhu, L. Xu, J. Chen, J. Shao, K. Han, W. Ma, Adv. Energy Mater. 8 (2018) 1801898.
[246] Z. Wei, J. Wang, Y. Liu, J. Yuan, T. Liu, G. Du, S. Zhu, S. Nie, Adv. Funct. Mater. 32 (2022) 2208277.
[247] W. Wang, P.F. Li, R. Xie, X.J. Ju, Z. Liu, L.Y. Chu, Adv. Mater. 34 (2022) 2107877.
[248] Y. Liu, J. Mo, Q. Fu, Y. Lu, N. Zhang, S. Wang, S. Nie, Adv. Funct. Mater. 30 (2020) 2004714.
[249] Z.-H. Lin, Y. Xie, Y. Yang, S. Wang, G. Zhu, Z.L. Wang, ACS nano 7 (2013) 4554.
[250] Y. Zhang, Z. Zhou, L. Sun, Z. Liu, X. Xia, T.H. Tao, Adv. Mater. 30 (2018) 1805722.
[251] S. Chun, C. Pang, S.B. Cho, Adv. Mater. 32 (2020) 1905539.
[252] L. Lin, Y. Xie, S. Wang, W. Wu, S. Niu, X. Wen, Z.L. Wang, ACS nano 7 (2013) 8266.
[253] R. Elnathan, N.H. Voelcker, Adv. Funct. Mater. 32 (2022) 2112100.
[254] S. Cheon, H. Kang, H. Kim, Y. Son, J.Y. Lee, H.J. Shin, S.W. Kim, J.H. Cho, Adv. Funct. Mater. 28 (2018) 1703778.
[255] S. Chen, T. Huang, H. Zuo, S. Qian, Y. Guo, L. Sun, D. Lei, Q. Wu, B. Zhu, C. He, Adv. Funct. Mater. 28 (2018) 1805108.
[256] Q. Gao, S. Agarwal, A. Greiner, T. Zhang, Prog. Mater. Sci. 137 (2023) 101139.
[257] Z. Huo, Y. Wei, Y. Wang, Z.L. Wang, Q. Sun, Adv. Funct. Mater. 32 (2022) 2206900.
[258] S. Roy Barman, Y.-J. Lin, K.-M. Lee, A. Pal, N. Tiwari, S. Lee, Z.-H. Lin, ACS nano 17 (2023) 2689.

Yongjiu Zou is an associate professor at College of Marine Engineering, Dalian Maritime University. He received his B.S. and M.S. in marine engineering both from Dalian Maritime University in 2012 and 2014, respectively. He spent a year as a visiting scholar at University of California, Los Angeles under the supervision of Prof. Jun Chen in 2020. His research focuses on triboelectric nanogenerators for energy harvesting and self-powered sensing.

Minzheng Sun received his B.S. from Dalian Maritime University in China in 2021. Currently, he is as a postgraduate student in Marine Engineering College, Dalian Maritime University. His current research work focuses on wind energy harvesting and self-powered sensing based on triboelectric nanogenerators.

Shuang Li received his B.S. from Dalian Maritime University in China in 2022. Currently, he is as a postgraduate student in Marine Engineering College, Dalian Maritime University. His current research work focuses on marine current energy collection and self-powered sensing based on triboelectric nanogenerators.

Xinyu Zhang received her B.S. from Shandong Jiaotong University in China in 2022. Currently, she is as a postgraduate student in Marine Engineering College, Dalian Maritime University. Her current research focuses on ocean energy harvesting and self-powered sensing based on triboelectric nanogenerators

Taili Du has been with Dalian Maritime University where he is currently an Associate Professor since 2010. He received his B. S. and M.S. from Dalian Maritime University in China in 2008 and 2010, and he is as a doctoral candidate in Marine Engineering College, Dalian Maritime University. His current research work focuses on vibration energy harvesting and self-powered vibration sensor based on Triboelectric Nanogenerator.

Minyi Xu received his Ph.D. degree from Peking University in 2012. During 2016–2017, he joined Professor Zhong Lin Wang' group at Georgia Institute of Technology. Now he is a Professor in the Marine Engineering College, Dalian Maritime University. His current research is mainly focused on the areas of blue energy, self-powered systems, triboelectric nanogenerators and its practical applications in smart ship and ocean.